Goldblatt, Ran; Deininger, Klaus W.; Hanson, Gordon H.

Article

Utilizing publicly available satellite data for urban research: Mapping built-up land cover and land use in Ho Chi Minh City, Vietnam

Development Engineering

Provided in Cooperation with:
Elsevier

Suggested Citation: Goldblatt, Ran; Deininger, Klaus W.; Hanson, Gordon H. (2018) : Utilizing publicly available satellite data for urban research: Mapping built-up land cover and land use in Ho Chi Minh City, Vietnam, Development Engineering, ISSN 2352-7285, Elsevier, Amsterdam, Vol. 3, pp. 83-99, https://doi.org/10.1016/j.deveng.2018.03.001

Development Engineering 3 (2018) 83–99

Contents lists available at ScienceDirect

Development Engineering

journal homepage: www.elsevier.com/locate/deveng

Utilizing publicly available satellite data for urban research: Mapping built-up land cover and land use in Ho Chi Minh City, Vietnam

Ran Goldblatt [a,*], Klaus Deininger [b], Gordon Hanson [a]

[a] University of California, San Diego, School of Global Policy and Strategy, 9500 Gilman Dr. La Jolla, CA 92093, USA
[b] World Bank, Washington DC, USA

ARTICLE INFO

Keywords:
Urbanization
Built-up land cover
Landsat
Sentinel
Google Earth Engine

ABSTRACT

Urbanization is a fundamental trend of the past two centuries, shaping many dimensions of the modern world. To guide this phenomenon and support growth of cities that are competitive and sustainably provide needed services, there is a need for information on the extent and nature of urban land cover. However, measuring urbanization is challenging, especially in developing countries, which often lack the resources and infrastructure needed to produce reliable data. With the increased availability of remotely sensed data, new methods are available to map urban land. Yet, existing classification products vary in their definition of "urban" and typically characterize urbanization in a specific point (or points) in time. Emerging cloud based computational platforms now allow one to map land cover and land use (LC/LU) across space and time without being constrained to specific classification products. Here, we highlight the potential use of publicly available remotely sensed data for mapping changes in the built-up LC/LU in Ho Chi Minh City, Vietnam, in the period between 2000 and 2015. We perform a pixel-based supervised image classification procedure in Google Earth Engine (GEE), using two sources of reference data (administrative data and hand-labeled examples). By fusing publicly available optical and radar data as input to the classifier, we achieve accurate maps of built-up LC/LU in the province. In today's era of big data, an easily deployable method for accurate classification of built-up LC/LU has extensive applications across a wide range of disciplines and is essential for building the foundation for a sustainable human society.

1. Introduction

Urbanization is a fundamental trend of the past two centuries and a key force in shaping many dimensions of the modern world. Between 1950 and 2014, the share of the global population living in urban areas increased from 30% to 54%; over the next few decades, the global urban population is projected to expand by an additional 2.5 billion individuals, primarily in Asia and Africa (UN, 2014). In the next 15 years alone, the global land area incorporated in cities is projected to grow by 1.2 million km^2 (Seto et al., 2012). While urbanization in rapidly growing nations is helping lift hundreds of millions of people out of poverty, it is also associated with immense societal challenges (Henderson, 2002). Unless guided by policies and appropriate planning, the speed and scale of urbanization in developing countries can result in unsustainable settlements that create pressure on ecosystems (Kontgis et al., 2014; Pham et al., 2015), a failure to effectively provide necessary public services (Cohen, 2006) and as a result, cities that are unable to compete in a globalized environment (Venables, 2017).

Countries of the Mekong region in Southeast Asia are transforming from rural to urbanized societies at a pace and scale never previously witnessed (Archer and Bezdecny, 2016). Vietnam, one of the most densely populated countries in the Mekong, has been urbanizing rapidly, both spatially and demographically, putting resources and basic services in peri-urban regions of the country under mounting strain (Saksena et al., 2014). The country has identified the promotion of a stable and sustainable urban development as a key element of its urban system master plan (Decision No. 445/QD-TTg, 2009) and spends considerable amounts of resources to generate, at 5-yearly intervals, information on land use. This information provides the basis for a wide range of policy decisions. In this paper, we propose a methodology that allows generation of such information based on satellite imagery in high precision and at any point in time. Accurate maps of LC/LU will allow monitoring changes on the ground at a much higher frequency compared to existing governmental data, which, in turn, may be of great value to policy makers.

How exactly do we measure urbanization? Previous literature

* Corresponding author.
E-mail address: rgoldblatt@ucsd.edu (R. Goldblatt).

https://doi.org/10.1016/j.deveng.2018.03.001
Received 18 October 2017; Received in revised form 21 February 2018; Accepted 19 March 2018
Available online 21 March 2018

characterizes urbanization, alternatively, as an increase in the share of the population living in cities, the level of non-agricultural employment or production, the pace of resource consumption, or the presence of traffic congestion (Yue et al., 2013). Data often come from census counts that are published infrequently and vary in their resolution and precision, due, it part, to limited resources for data collection (Keola et al., 2015).

Since the 1970s, terrestrial Earth-observation data have been collected in various spectral, spatial and temporal resolutions. With the increased availability of satellite imagery and other types of remotely sensed data, new methods are being developed to convert these data into meaningful information about the nature and pace of change of urban landscapes and human settlements (Ban et al., 2015; CIESIN, 2005; Chen et al., 2015; Gaughan et al., 2013; Pesaresi et al., 2016b; Potere et al., 2009; Seto et al., 2011; Taubenböck et al., 2012). Reliable and accessible tools that utilize publicly available satellite data to map and measure urbanization across both space and time would help developing countries to promote a sustainable urban development.

Covering a period of over 40 years, Landsat satellites provide the longest temporal record of moderate resolution multispectral data of Earth's surface. Because Landsat satellites have been collecting data from Earth since 1972, these data are often used for analysis of urbanization (Patel et al., 2015; Seto et al., 2011). However, the moderate spatial resolution (30 m) of Landsat does not allow one to fully capture the complex spatial patterns of urban environments (Lu et al., 2010), due, in part, to the problem of "mixed pixels," i.e., the spectral reflectance mixture of different land cover classes within a pixel (Lee and Lathrop, 2005). The launch of the European Space Agency's Copernicus program Sentinel satellites in the mid-2010s, represents a major advance in the public availability of remotely sensed data. Sentinel satellites provide global coverage of radar and multi-spectral imaging instruments for land, ocean and atmospheric monitoring with high-resolution observations and a high revisit rate. Although the added value of Sentinel-derived data for classification of land cover and land use has been shown in past research (Forkuor et al., 2017; Pesaresi et al., 2016a; Sharma et al., 2017), the potential combined use of Sentinel-1 and Sentinel-2 data for urban research remains underexplored.

In this study, we demonstrate the use of different sources of publicly available remotely sensed data for mapping the built-up land cover and land use (LC/LU) in one province in Vietnam - Ho Chi Minh City. We perform the classification in Google Earth Engine (GEE), a cloud-computing platform for planetary-scale analysis. GEE has been previously used, for example, to map population (Patel et al., 2015; Trianni et al., 2015), urban extent (Goldblatt et al., 2016, 2018), and surface water (Pekel et al., 2016). We show that with publicly available satellite data and open-access cloud-based computational platforms, it is now possible to map LC/LU with high precision and high temporal resolution. We perform supervised pixel-based image classification utilizing two sources of reference data (ground-truth labeled examples): high-resolution administrative cadastral data from the Vietnamese government and hand-labeled examples. We use these data to map changes in the extent of built-up LC/LU in the period between 2000 and 2015 and evaluate the relation between the extent of built-up LC/LU, population size and economic development (measured according to the intensity of light emitted at night). Our objective is not to propose a new classification product or to develop a new machine learning approach but to validate the use of a low-cost, publically available tool for analyzing the pace of LC/LU change for a wide-range of geographical scales.

To summarize, the objectives of this study are: (1) to present a reliable, low-cost tool that uses publicly available satellite data and cloud-based computational platform to map built-up LC/LU in HCMC, Vietnam; (2) to map temporal changes in the extent of built-up land cover in the province, over the period 2000 to 2015; (3) to evaluate the use of administrative vector data as reference for supervised image classification; and (4) to evaluate the association between the extent of built-up land cover and the distribution of the population and economic activity in the province.

We now provide a description of previous studies utilizing remotely sensed data for urban research, including in the context of Vietnam (Section 2). We then turn to describe the study area and the research methods (Section 3). In section 4 we present and evaluate the results. In Section 5, we offer a concluding discussion.

2. Background

2.1. Measuring urbanization by means of remote sensing

Urbanization occurs as rural areas are incorporated into cities, typically through sprawl radiating out from the city center or linearly along major transportation corridors (Baum-Snow, 2007; Sudhira et al., 2004). The growth of cities, which often occurs in unplanned and uneven patterns (Sudhira et al., 2004), changes the spatial distribution of population sub-groups (Rahman et al., 2011), often together with altering LC/LU patterns (Bhatta, 2009; Schneider et al., 2010) including through the expansion of built-up areas and impervious surfaces (Bhatta, 2009; Jat et al., 2008) and the conversion of farmland into urban settlements (Dewan and Yamaguchi, 2009).

Remotely sensed data, which record the physical characteristics of Earth, can be used to measure the spatial-physical characteristics of urban environments, such as impervious surfaces (Lu and Weng, 2006; Slonecker et al., 2001; Weng, 2012), street networks (Hu et al., 2014; W. Shi et al., 2014b; Zhang et al., 2002), building footprints (Lu et al., 2014; Taubenböck and Kraff, 2014; Zeng et al., 2013) and urban green spaces (Feyisa et al., 2014; Rotem-Mindali et al., 2015), and to map urbanization processes (Patino and Duque, 2013). An extensive body of research has utilized publicly available remotely sensed data for urban research, including data acquired by Landsat (Chen et al., 2015; Gaughan et al., 2013; Goldblatt et al., 2016; Patel et al., 2015), MODIS (Moderate Resolution Imaging Spectroradiometer) (Schneider et al., 2010; Wan et al., 2015), DMSP-OLS (Elvidge et al., 2014; Liu et al., 2012; Xiao et al., 2014; Zhang and Seto, 2013), VIIRS (Elvidge et al., 2013, 2017) and other HR, VHR and SAR radar sensors (Ban et al., 2015; Chen et al., 2013).

The accuracy of the classification – or, the successful mapping of LC/LU by means of machine learning – depends largely on the properties and characteristics of the input data that are used for classification. These characteristics include the *spatial resolution* of the sensors (i.e., the size of the smallest object that can be identified as an individual entity), their *spectral resolution* (i.e., the number of spectral bands, their bandwidths and locations along the spectrum (Herold et al., 2003) and the *temporal resolution* of the acquired data (i.e., the revisit period of the satellite in a given location on Earth).

Spatial resolution is considered one of the most significant factors in determining the successful mapping of heterogeneous and fragmented landscapes (Chen et al., 2004), including complex urban settings (Herold et al., 2002; Momeni et al., 2016; Rashed and Jürgens, 2010; Sertel and Akay, 2015). In addition, specific spectral bands, such as thermal bands, can improve classification performance in urban environments. For example, because industrial and dense urban areas are warmer than open farmland and or natural vegetation (Roth et al., 1989), using these bands as input for classification can increase the separability of these land cover types.

Yet, choosing which data to use and for which application depends on the characteristics of the data, its coverage, availability and cost, as well as on the methods used to interpret and analyze the data (Pohl and Genderen, 1998). Different sensors record distinct characteristics of the surface (e.g., brightness, temperature, height, density, texture), but not always at the same resolution. Because each of these characteristics can improve our understanding of land cover, data fusion techniques that exploit the best characteristics of each type of sensor have become a valuable procedure in remote-sensing analysis (Abdikan et al., 2014), including for urban applications (Gamba, 2014). For example, urban settings are often characterized by complex textures, compositions and heights. These features can be captured by Synthetic Aperture Radar

(SAR) sensors, such as those on board Sentinel-1 (Koppel et al., 2015). Furthermore, combining optical and radar data through data fusion (e.g., by infusing Sentinel-1 SAR data with Landsat or with Sentinel-2) allows one to extract information about the reflectance of the surface, in addition to its geometry and texture (Haack et al., 2000) and to improve the accuracy of classification of built-up areas (Fonteh et al., 2016; Pesaresi et al., 2016a). For example, Amarsaikhan et al. (2010) have shown that multi-source information can significantly improve the interpretation and classification of land cover types of urban features and improve that accuracy of urban land cover classification. More generally, data fusion is the process of combining diverse types of information from a wide variety of sensors to increase the accuracy of the data and its utility (Pohl and Genderen, 1998), which, in turn, improves decision making and initiate actions (Goodman et al., 2013). Data fusion can be classified into three levels: pixel, feature/object, and knowledge/decision (Pohl and Genderen, 1998), where pixel-based fusion provides the best potential for keeping the original information of the input images in the merged output data (Abdikan et al., 2014).

With the increased availability of remotely sensed data, much effort has been put towards converting these data into meaningful information about the characteristics of land cover and land use on Earth. However, until recently, most remote sensing studies have focused on local settings (Herold, 2009). This is because mapping land cover at a national or regional scale is challenging due to the lack of high-resolution global imagery, the spectral heterogeneity and complexity of land, the small and fragmented spatial configuration which characterizes many cities (Chen et al., 2015; Herold, 2009), as well as due to the lack of reference data and other computational constraints. While these studies map the land cover and land use with high precision in local settings, their transferability to other regions is unknown and potentially problematic (Kii and Nakamura, 2017).

In the last decade, several classification products have been developed to map urban land and the human footprint, globally. The Global Human Settlement Layer (GHSL) (Pesaresi et al., 2013) characterizes human settlements and building structures in four points in time (1975, 1990, 2000, 2015) based on optical sensors in a spatial resolution of 0.5–10 m. The Global Urban Footprint (GUF) (Esch et al., 2017) of the German Aerospace Center (DLR) characterizes built-up areas at approximately 12 m spatial resolution, based on satellite imagery acquired between 2011 and 2012. The Global Man-made Impervious Surface (GMIS) (de Colstoun et al., 2017) estimates global fractional impervious cover derived from 2010 GLS Landsat data. The Global Land Cover database for the year 2000 (GLC2000) (Bartholomé and Belward, 2005) characterizes 22 types of types of land-cover, including artificial surfaces (built-up land cover), based on data collected from SPOT 4.

While these and other datasets provide essential information about urbanization, they typically characterize urbanization in a specific point (or points) in time. Promoting sustainable development requires monitoring urbanization in high frequency without being constrained by the specific characteristics of existing products (e.g., their frequency, spatial resolution, definition of urbanization, etc.).

As we show in this study, emerging cloud based computational platforms, such as Google Earth Engine (GEE), allow any user to classify the land cover in any place in the world and at any point in time. Here, we demonstrate the use of GEE for mapping the built-up LC/LU in Ho Chi Ming City, Vietnam across time.

2.2. Urbanization in Vietnam

Vietnam (approximately 330 km^2 in size) is one of the most densely populated countries in the world (96 million people in 2018). The majority of the population concentrates along the South China Sea and Gulf of Tonkin, especially in the Mekong Delta (in the south) and the Red River Valley (in the north). Over the past few decades, Vietnam has undergone rapid urbanization (Arouri et al., 2017; Kontgis et al., 2014; Pham and Yamaguchi, 2011) together with significant changes in land cover and land use patterns (Pham et al., 2015). Since 1990, the share of its population living in urban areas increased from 20% to 33.6%, due primarily to rural-urban migration and an increase in non-farm economic activities (Arouri et al., 2017). By 2025, 450,000 ha of agricultural land are expected to be converted into urban land to accommodate 52 million urban dwellers (Decision No. 445/QD-TTg, 2009). These changes impose immense environmental (Béland et al., 2006; Dasgupta et al., 2005; Swetnam et al., 2011; Ziegler et al., 2007) and societal (Castella et al., 2007; Trincsi et al., 2014) challenges to the country.

In this study, we map built up LC/LU in Ho Chi Minh City (HCMC). HCMC, 2098.7 km^2 in size, is located in the Mekong Delta (Fig. 1). It is the largest urban agglomeration in the country and the nation's financial capital and economic hub, due, partly, to its proximity to a deep-water port (Vietnam Urbanization Review: Technical Assistance Report, 2011). Between 1975 and 2015, the city's population increased from 3.0 million to 8.2 million inhabitants and is expected to reach 9.2 million inhabitants in 2020 and 10.0 million in 2025 (Triet and Phu, 2014). Between 1990 and 2012, 660.2 km^2 of cropland were converted to urban areas and the built-up area increased by 4.8 times, with one-third of the expansion occurring more than 40 km from the city's urban core (Kontgis et al., 2014). The city's development has taken place in conflict with 'official' planning policies, which has created vulnerability to flood risks from surrounding wetlands (Nguyen et al., 2016). HCMC is one of seven cities facing the greatest risk from the onset of climate change related hazards (Maplecroft, 2012). Understanding the rapid urbanization processes in HCMC is critical for efficient urban planning (Son et al., 2012) and for the maintenance of a sustainable development in Vietnam.

Much effort has been put to construct and maintain a digitized, up-to-date cadastral database (Decision No. 445/QD-TTg, 2009) and to map the land cover and land use in the country. Currently, two sources provide official data on the distribution of land-use in Vietnam; one for forest management (used by the Ministry of Agriculture and Rural Development (MARD)) and one for land use planning and management (used by the General Department of Land Administration (GDLA) of the Ministry of Natural Resources (MONRE)) (van Dijk et al., 2013). The latter provides a basis for planning, economic and social development, and the determination of land prices (Quang Hien et al., 2015). Digital data on urbanization in Vietnam, however, remain sparse (Saksena et al., 2014), and there is an increasing need for methods to promote efficient and accurate cadastral survey and mapping (Bojo, 2011).

3. Methods

3.1. Reference data for supervised image classification

Automatic classification of LC/LU requires reference data for training and (or) validation, specifically, reference data that mark urban features are necessary for mapping urban areas. Previous studies utilize census-based population databases (Stevens et al., 2015), hand-labeled examples (Goldblatt et al., 2016) and data collected via crowd-source platforms, such as OpenStreetMap (OSM) (Belgiu and Drăguţ, 2014; Estima and Painho, 2015) as reference for supervised image classification. However, because they are expensive to collect, large-scale reference datasets are scarce (Miyazaki et al., 2011). Here, we use two types of reference data for supervised pixel-based image classification: GDLA administrative cadastral data (polygons) and hand-labeled examples (points).

3.1.1. GDLA land use classification

Administrative cadastral data were obtained from the Vietnam

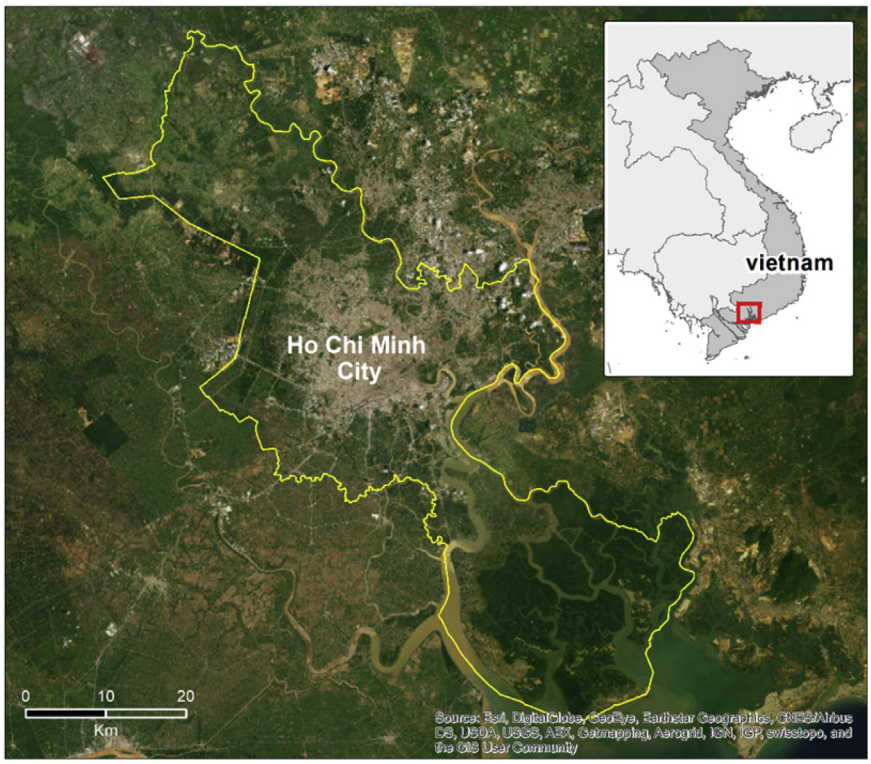

Fig. 1. Ho Chi Minh City province.

Table 1
Our categorization of GDLA LC/LU as "not-built-up" land cover, "residential" and "non-residential" land use.

1. Built-up land cover	2. Non built-up land cover
1a. Non-residential Land use	• Unused delta land
• Telecommunication	• Flat annual crop land
• Historical vestige	• Annual crops
• Education	• Perennial crops
• Roads	• Unused land
• Power supply	• Unused hilly and mountain land
• Sport activities	• Land for irrigation systems
• Public services	• Rice cultivation
• Health services	• Paddy rice land for 2 crops/year
• Cemeteries, graveyard	• Remaining rice land
• Industrial area	• Water surface
• Worship	• Agricultural land
• Institutions/organizations	• Aquaculture
• Offices, headquarters and non-profit agencies	• Special-use forest
1b. Residential Land use	• Production forest
• Urban residential land	• Rivers, canals, streams
• Urban residential land	• Agricultural production

General Department of Land Administration (GDLA) of the Ministry of Natural Resources and Environment (MONRE) overlaid with cadastral data.[1] The data consists of 72,501 polygons that span Ho Chi Minh City. Each polygon is marked by its LC/LU type. We categorize LC/LU types as either "built-up" (BU) or "not-built-up" (NBU). Additionally, we categorize each type of BU land cover as either "residential" (urban or rural residential) or as "non-residential" land use (Table 1 and Fig. 2). From the 72,501 polygons, we select a random sample of 6300 polygons: 4000 BU polygons (2000 residential and 2000 non-residential) and 2300 NBU polygons. These polygons cover 73.2 km^2 of built-up areas and 77 km^2 of not-built-up areas.

3.1.2. *Hand-labeled examples*

GDLA characterizes continuous areas (polygons) of relatively homogenous LC/LU types. Because we perform classification at the level of the pixel, there is a risk of "class noise," i.e., polygons that consist of pixels that belong to different LC/LU types. We therefore create an additional reference dataset consisting of 15,945 points, which we hand-label as one of three classes: "BU residential", "BU non-residential", or "NBU". We sample these points from across the universe of the 6300 GDLA polygons. We overlay the points with Google Earth high-resolution base map and manually determine the LC/LU of the points using a visual interpretation method. First, we label the points as either "built-up" (i.e., a paved or human-made surface) or as "not-built-up" (absence of paved or other human-made surface). Then, we label each "built-up" point as "residential" or as "non-residential". Because it is impossible to differentiate visually between residential and non-residential land use, we determine the land use of each "built-up" point according to the land use class of the overlapping GDLA polygon. Three graduate students, who were provided with extensive training and supervised by the researchers, manually labelled the points. We provided each student an equal proportion of samples. The students labeled each point by a visual interpretation of the most recent available satellite image (typically from 2015 to 2017). 5115 points are labeled as "not built-up", 4385 points are labeled as "built-up residential" and 6445 points are labeled as "built-up non-residential" (Fig. 3 presents the spatial distribution of the hand-labeled examples).

3.2. *Classifiers input*

We evaluate four types of inputs to the classifier: (1) Landsat 8; (2) Sentinel-2; (3) Sentine-1; and (4) Sentinel-2 and Sentinel-1 combined (in

[1] GDLA was established by the Vietnam Government in 1994 and is responsible for the preparation of land legislation and land policies, implementation of cadastral system, land statistics and current land use and land rights mapping.

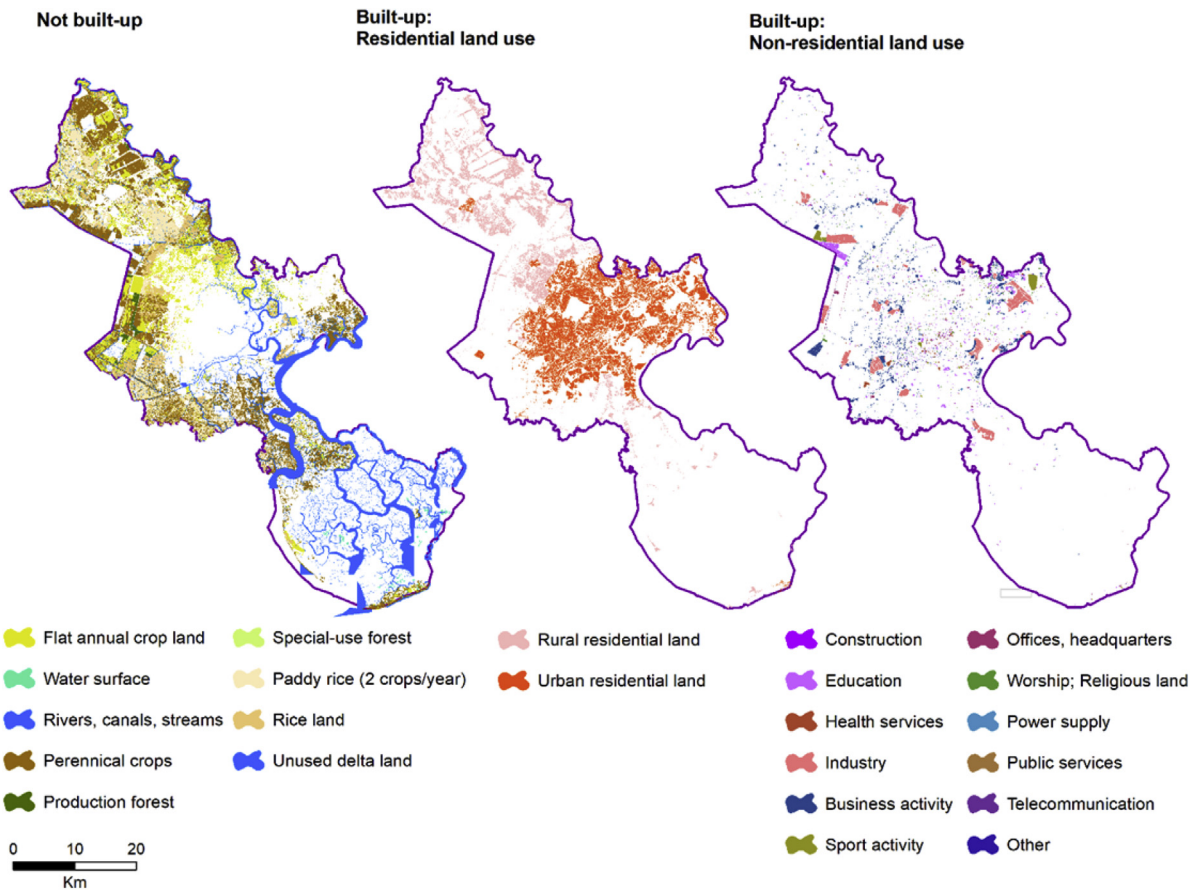

Fig. 2. Our categorization of GDLA cadastral data as built-up residential land-use, built-up non-residential land-use and not-built-up land cover.

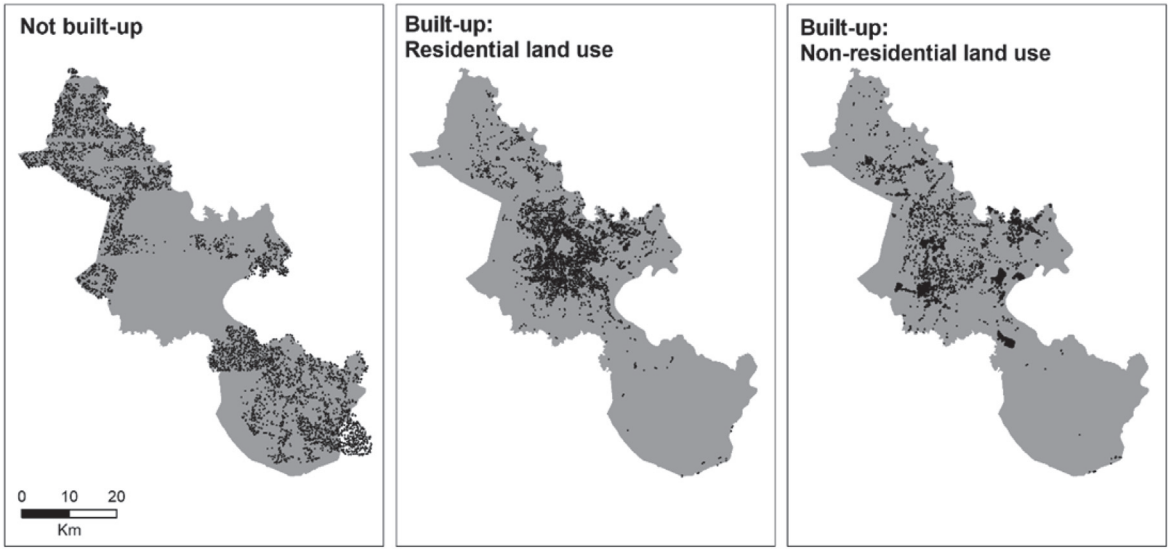

Fig. 3. The distribution of the hand-labeled examples (points). 15,945 points were hand-labeled as either "not built-up", "built-up residential" or as "built-up non-residential".

which each pixel includes the band values of both Sentinel-2 and Sentinel-1).

3.2.1. *Landsat 8*

Landsat 8 covers the entire globe every 16 days and collects data with eleven spectral bands, nine in a spatial resolution of 15 m–30 m, and two in a spatial resolution of 100 m (Table 2). We apply a standard Top-of-Atmosphere (TOA) calibration to all USGS Landsat 8 Raw Scenes in 2015. We assign a "cloud score" to each pixel and select the lowest possible range of cloud scores (less than 10 per cent cloud coverage). The cloud score is a simple cloud-likelihood score which is determined according to the brightness of a pixel, its temperature, and a computed per-pixel Normalized Difference Snow Index (NDSI). We compute per-band median values from the accepted pixels. Per-pixel median values are

Table 2
The spectral bands of Landsat 8 and Sentinel-2.

	Landsat-8		
	Spectral band	Wavelength (micrometers)	Resolution (meters)
B1	Band 1 – Ultra blue	0.43–0.45	30
B2	Band 2 - Blue	0.45–0.51	30
B3	Band 3 - Green	0.53–0.59	30
B4	Band 4 – Red	0.64–0.67	30
B5	Band 5 - Near Infrared (NIR)	0.85–0.88	30
B6	Band 6 - SWIR 1	1.57–1.65	30
B7	Band 7 - SWIR 2	2.11–2.29	30
B8	Band 8 - Panchromatic	0.50–0.68	15
B9	Band 9 – Cirrus	1.36–1.38	30
B10	Band 10 - Thermal Infrared (TIRS) 1	10.60–11.19	100 (resampled to 30)
B11	Band 11 - Thermal Infrared (TIRS) 2	11.50–12.51	100 (resampled to 30)
	Sentinel 2		
	Spectral band	**Wavelength (nm)**	**Resolution (meters)**
B1	Aerosols	443	60
B2	Blue	490	10
B3	Green	560	10
B4	Red	665	10
B5	Red Edge 1	705	20
B6	Red Edge 2	740	20
B7	Red Edge 3	783	20
B8	NIR	842	10
B8a	Red Edge 4	865	20
B9	Water vapor	940	60
B11	SWIR 1	1610	20
B12	SWIR 2	2190	20

insensitive to extreme values, such as very bright or dark pixels, in a stack of scenes (Flood, 2013). For display purposes, we scale the decimal value of each pixel to an 8-bit range (0–255).

3.2.2. Sentinel-1

Sentinel-1 is a polar-orbiting, all-weather, day-and-night radar imaging mission, which captures the entire Earth every six days. Sentinel-1 carries an advanced synthetic aperture radar (SAR) that includes C-band imaging, which is well suited for capturing the structure and density of urban environments (Koppel et al., 2015). We use the VV mode (single co-polarization, vertical transmit/vertical receive). Each scene is pre-processed, including speckle noise removal, radiometric calibration and terrain correction. Sentinel-2 is a wide-swath, high-resolution, multi-spectral imaging mission. It samples 13 spectral bands: four bands at 10 m, six bands at 20 m and three bands at 60 m spatial resolution (Table 2). We select all scenes in 2016 with less than 10 per cent cloud coverage and calculate per-pixel per-band median value.

3.2.3. Additional spectral indices

Previous studies show that the addition of non-linear spectral indices as inputs to a classifier improve the classifier's performance (Goldblatt et al., 2016). Therefore, for each Landsat 8 and Sentinel-2 pixel we calculate five additional indices, which we use as additional predictors to the classifier: Normalized Difference Vegetation Index (NDVI) (Pettorelli et al., 2005), Normalized Difference Water Index (NDWI) (McFeeters, 1996), Urban Index (UI) (Kawamura et al., 1996), Enhanced Vegetation Index (EVI) (Jiang et al., 2008) and Normalized Difference Built-up Index (NDBI) (Zha et al., 2003).

3.3. Classifier

We perform per-pixel supervised image classification with Random Forest as the classifier. Random Forests are tree-based classifiers that include k decision trees (k predictors). When classifying an example, its variables are run through each of the k tree predictors, and the k predictions are averaged to obtain a less noisy prediction (by voting on the most popular class). The learning process of the 'forest' involves some level of randomness; each tree is trained over an independent random sample of examples from the training set and each node's binary question in a tree is selected from a randomly sampled subset of the input variables. We choose to use Random Forest because previous studies find that the performance of Random Forest is superior to other classifiers (Goldblatt et al., 2016), especially when dealing with large-scale, noisy and high dimensionally dataset, and because the routine is robust to outliers (Gislason et al., 2006). Random Forests are computationally lighter than other tree ensemble methods (Jean et al., 2016; Rodriguez-Galiano et al., 2012) and can effectively incorporate many covariates with minimum tuning and supervision (Stevens et al., 2015). Specifically in the remote sensing domain, Random Forests often achieve high accuracy rates for classification of hyperspectral, multispectral, and multisource data (Guan et al., 2013). We set the number of trees in the Random Forest classifier to 20. Previous studies show mixed results as for the optimal number of trees in the decision tree. The number ranges between 10 trees (Zhang et al., 2012) and 100 trees (Rodriguez-Galiano et al., 2012). According to Goldblatt et al. (2016), although the performance of Random Forest improves as the number of trees increases, this pattern holds only up to 10 trees and the performance remains nearly the same with 50 and with 100 decision trees.

3.4. Accuracy assessment

First, we post process the classified images to remove pixels that were classified as built-up and that are characterized by a high NDVI value (a visual inspection shows that a threshold of 0.3 is sufficient to remove misclassified vegetation pixels). We then assess the accuracy of classification.

Different approaches can be employed to evaluate the accuracy of a classification task. An error matrix approach is commonly used to assess, describe and report the accuracy of classification into categorical classes (Lu and Weng, 2007). It expresses the number of sample units assigned to a given category relative to the number of the classified sample units and can be used to calculate to general types of erros: *commission errors* (i.e., examples that were wrongly classified as belonging to a given class) and *omission errors* (examples that were wrongly not classified as belonging to a given class). In addition, the error matrix can be used to calculate accuracy measures. The most commonly reported statistic for accuracy assessment is *overall accuracy*, which implies the ratio between the number of correctly classified sample units and the number of all sample units (Congalton and Green, 2008). *Producer's accuracy (*or, *true-positive rate)* and *user's accuracy* describe the accuracy of individual categories instead of the overall classification accuracy (i.e., the probability that true positive and true negative examples are correctly classified, respectively). *True-negative rate* (or *specificity*) describes the percentage of actual negative examples classified correctly as negative. Although producer's and user's accuracies are standard practice in a two-class classification problem, *balanced accuracy rate* is also important especially when dealing with imbalanced two-class datasets (the measure describes the average between Producer's accuracy and true-negative rate.

We evaluate the accuracy of the classification using confusion matrixes, which compare the predicted (classified) classes of the examples in the test set with their actual class (resulting in four possible combinations: TP (True-positive), TN (True-negative), FP (False-positive) and FN (False-negative)). We assess the accuracy of the classification according to the following performance estimators (we refer to the classes "built up" (BU) and "built-up residential" as positive and to the classes "not built-up" (NBU) and "built-up non-residential" as negative):

(1) Producer's accuracy, referred to as True-Positive Rate (TPR) (the percentage of actual positive examples classified correctly as positive); (2) True-Negative Rate (TNR) (the percentage of actual negative examples classified correctly as negative); (3) Balanced Accuracy (the average

of TPR and TNR); (4) User's accuracy (the percentage of correctly classified positive examples of all examples predicted as positive):

1. Producer's accuracy (TPR) = TP/(TP + FN)
2. TNR = TN/(TN + FP)
3. Balanced Accuracy = (TPR + TNR)/2
4. User's accuracy = TP/(TP + FP)

Where TP is the number of the actual positive examples predicted to be positive; TN is the number of negative examples predicted as negative; FN is the number of actual positive examples predicted as negative and FP is the number of actual negative examples predicted as positive.

The performance, or the accuracy, of a classifier refers to the probability that it will correctly classify a random set of examples. To assure a "fair" assessment of a classifier's generalization, the data used to train the classifier (training set) must be separated from the data that are used to assess its accuracy (test set). Different data splitting heuristics can be used to assure separation between the training and test sets (Kohavi, 1995), including the holdout method, in which the data is divided into two mutually exclusive subsets: a training set and a test/holdout set; bootstraping, in which the dataset is sampled uniformly from the data, with replacement; and cross-validation, also known as *k*-fold cross-validation, in which the data are divided into *k* subsets (optimally 5 or 10, to allow a less biased estimation (Rodriguez et al., 2010)) with *k* "experiments". The cross-validation procedure ensures that each example is included exactly once in the test fold and that each example in the test fold is not used to train the classifier. Averaging the overall accuracy across all *k* partitions yields *k* accuracy values, or *k* hold-out estimators, and a variance estimation of the classification error (Arlot and Celisse, 2010; Salzberg, 1997). Though each of these methods can be used to assess the performance of a given classifier, cross-validation is a widely accepted procedure (Refaeilzadeh et al., 2009) that provides a robust estimate of a classifier's generalization error (Blum et al., 1999). When the instances are representative of the underlying population and when sufficient instances are available for training, this procedure results in an unbiased estimate of the accuracy of the classifier over the population (Bradford and Brodley, 2001).

In this study, we adopt a *k*-fold cross-validation procedure (with *k* "experiments") to estimate the accuracy of the classifiers. In each experiment, the examples in one of the data folds are left out for testing and the examples in the remaining *k*-1 folds are used to train the classifier. The performance quality of the trained classifier is tested on the left-out fold, and the overall performance measure is then averaged over the *k* folds (over the k experiments). Note, that the examples in the reference data are divided into five folds and each example—and all examples—are tested exactly once. The reported matrixes describe the predicted class against the "real" class of all examples across the five folds (i.e. across the five experiments).

3.5. Built-up land cover as the distribution of the population

To assess the relation between the extent of built-up land cover and the distribution of the population in Ho Chi Minh City we really on two commonly used measures for population distribution: census-based population counts (according to the 2015 Population and Labor Statistics[2]) and the intensity of the light emitted at night (as it is measured by DMSP-OLS and by VIIRS).

Previous studies show that the intensity of light emitted at night (referred to as nighttime light) is highly correlated with developed land (Elvidge et al., 2014; Levin and Duke, 2012; Sutton, 2003) and can be used to infer the extent of urban areas (Bagan and Yamagata, 2015; Small and Elvidge, 2013; Zhang and Seto, 2013), as well as economic activity at the local, regional and national levels (Elvidge et al., 2014; Henderson et al., 2003; Keola et al., 2015). Thus, the extent and intensity of nighttime light provides a reasonable proxy for estimation of the spatial distribution of urban areas. Previous studies find a clear association between the spatial distribution and intensity of nighttime light and urbanization (Small and Elvidge, 2013), including changes in the distribution of urban land use, at local, regional, and national levels (Bagan and Yamagata, 2015). The intensity of nighttime light is also related to population dynamics (Bagan and Yamagata, 2015; Pandey et al., 2013), economic activity and GDP (Elvidge et al., 2014; Henderson et al., 2012; Laveesh Bhandari and Roychowdhury, 2011). We measure the intensity of nighttime light that is captured by DMSP-OLS and VIIRS.

3.5.1. DMSP-OLS

The Operational Line-scan System of the Defense Meteorological Satellite Program (DMSP-OLS) has been capturing artificial lighting since the early 1990's, making it the longest continuous remote sensing product for global time series analysis of urbanization (Elvidge et al., 2014). We use version 4 of the DMSP-OLS Nighttime Lights Time Series, which consists of cloud-free composites made using all the available archived DMSP-OLS smooth resolution data for calendar years. We use the "stable lights" band, which contains the lights from cities, towns, and other sites with persistent lighting, excluding gas flares. Ephemeral events, such as fires are discarded. The background noise is identified and replaced with values of zero. Because DMSP-OLS calibrated and processed data are only available until 2013, we use the data captured by 'F182013' satellite.

3.5.2. VIIRS

Since 2012, the Visible Infrared Imaging Radiometer Suite (VIIRS) sensors have been capturing remotely sensed data, including at nighttime. VIIRS provides several key improvements over DMSP-OLS data (Small et al., 2013), including a vast reduction in the pixel footprint, uniform GIFOV (ground instantaneous field of view) from nadir to edge of scan, lower detection limits, wider dynamic range, finer quantization, and in-flight calibration (Elvidge et al., 2017). We use the VIIRS Day/-Night Band (DNB) product, which excludes data impacted by cloud cover.

We perform the analysis at the geographical level of the district. For each district in Ho Chi Minh City we calculate the sum of the intensity of light of all (DSMP-OLS or VIIRS) pixels (referred to as SOL), the total number of people and the total area of built-up land cover (we apply a $\log_{10}$ reduction). For all measures, we weight by the area of the district.

4. Results

4.1. Using GDLA as reference for supervised image classification

We begin the analysis with GDLA as reference for the classifier. As explained above, we use a stratified random sample of 6300 polygons that we categorize as "built-up residential", "built-up non-residential" or "not built-up". We overlap the polygons with the satellite data (the input) and assign each pixel with a corresponding label. We evaluate the classification with four types of inputs to the classifier: Landsat 8 (L8), Sentinel-1 (SE1), Sentinel-2 (SE2) and a combination of Sentinel-1 and Sentinel-2 (SE1SE2). Following training, the classifiers predict for each new example (pixel), the probability (a posterior probability in the range between 0 and 1) that it is "built-up". We characterize a pixel as "built-up" if the probability it is "built-up" exceeds a threshold of 0.5. We find, that SE1SE2 as input to the classifier results in the best performance, indicated by a high balanced accuracy of 80% (compared to 75% and 62%, with SE2 and SE1 as input to the classifiers, respectively). Classification with L8 results in the lowest balanced accuracy (73%) (Table 3).

We also evaluate the performance of the classifiers in differentiating between residential and non-residential land use. For evaluation

[2] The 2015 Population and Labor statistics of the Statistical Office in Ho Chi Minh City http://www.pso.hochiminhcity.gov.vn/c/document_library/get_file?uuid=7311d5ad-c5a4-4383-8fb4-36c209afa120&groupId=18.

Table 3
Performance measures and confusion matrixes: classification of built-up vs. not built-up (top) and residential vs. non-residential pixels (bottom) (reference data: GDLA).

	L8				SE2				SE1				SE1SE2			
	built-up and not-built-up															
			predicted				predicted				predicted				predicted	
			BU	NBU			BU	NBU			BU	NBU			BU	NBU
	actual	BU	65956	17340	actual	BU	63546	16223	actual	BU	52495	27274	actual	BU	66423	13346
		NBU	23343	49906		NBU	22409	50527		NBU	31196	41740		NBU	17316	55620
Overall	73.5%				74.7%				61.7%				79.9%			
Producer's	78.4%				79.7%				65.8%				83.3%			
TNR	68.1%				69.3%				57.2%				76.3%			
Balanced	73.3%				74.5%				61.5%				79.8%			
User's	73.0%				73.9%				62.7%				79.3%			
	residential and non-residential															
			predicted				predicted				predicted				predicted	
			Res	NRes			Res	NRes			Res	NRes			Res	NRes
	actual	Res	26073	14206	actual	Res	22027	18154	actual	Res	27135	13046	actual	Res	27942	12239
		NRes	16676	23341		NRes	18780	20808		NRes	14349	25239		NRes	13415	26173
Overall	61.5%				65.7%				53.7%				67.8%			
TPR	64.7%				67.5%				54.8%				69.5%			
TNR	58.3%				63.8%				52.6%				66.1%			
Balanced	61.5%				65.6%				53.7%				67.8%			
Precision	61.0%				65.4%				54.0%				67.6%			

purposes, we define a "positive" example as "residential" and a "negative" example as "non-residential". We find relatively poor performance when classification is performed with L8 as input to the classifier, indicated by a balanced accuracy of approximately 62%. Classification with SE1SE2 as input to the classifier outperforms classification with the other inputs; the balanced accuracy increases from 62% with L8 to 68% with SE1SE2. Classification with SE1 as a single input to the classifier also exceeds chance level (a balanced accuracy of 54%).

4.2. Using the hand-labeled examples as reference for supervised image classification

The classification we perform in this study is at the level of the pixel (i.e., the classifier is trained with "labeled" pixels and predicts the class of new pixels). In the previous experiment, we used GDLA as the reference, where each polygon is characterized by a single LC/LU class, assuming relatively homogenous pixels within a polygon. Because we assign a label to each pixel according to the class of an overlapping polygon, there is a

Table 4
Spectral profile (Sentinel-2) of not-built up (NBU), residential and non-residential pixels and a comparison of means.

		NBU	Residential	Non-Residential		*t*-test[a] (BU/NBU)	*t*-test[a] (Residential/non-residential)
B1	Mean	1454.496	1840.1604	1807.0469	t	−1.2e+02	8.7021
	Std. error	1.674642	2.347501	2.701971	p	0.0000	0.0000
B2	Mean	1177.891	1636.931	1604.958	t	−1.1e+02	5.9762
	Std. error	2.065869	2.921192	3.940023	p	0.0000	0.0000
B3	Mean	1056.124	1521.83	1509.729	t	−98.6353	1.9748
	Std. error	2.276774	3.073889	4.601121	p	0.0000	0.0483
B4	Mean	844.3438	1509.181	1468.387	t	−1.1e+02	5.3144
	Std. error	3.403674	3.862232	5.760496	p	0.0000	0.0000
B5	Mean	975.7462	1517.389	1517.218	t	−1.1e+02	0.0270
	Std. error	3.076735	2.88339	4.834245	p	0.0000	0.9785
B6	Mean	1640.949	1888.244	1988.923	t	−39.7245	−16.2751
	Std. error	9.181004	2.93428	4.695726	p	0.0000	0.0000
B7	Mean	1976.419	2122.081	2278.861	t	−24.2797	−21.5834
	Std. error	12.06896	3.832173	5.394515	p	0.0000	0.0000
B8	Mean	1818.344	1907.858	2091.06	t	−20.5193	−25.5771
	Std. error	11.80957	3.900075	5.278707	p	0.0000	0.0000
B8A	Mean	2134.658	2249.111	2474.616	t	−21.1651	−27.1744
	Std. error	14.58746	2474.616	6.116062	p	0.0000	0.0000
B9	Mean	−2.216958	−1.400443	-.6386438	t	−16.1045	−16.7963
	Std. error	.2062281	.7573329	.2777427	p	0.0000	0.0000
B10	Mean	9.252884	11.72212	11.67983	t	−1.0e+02	1.7509
	Std. error	.0235133	.0166123	.0164072	p	0.0000	0.0800
B11	Mean	1136.883	2213.7	2278.581	t	−1.2e+02	−6.9082
	Std. error	10.11071	4.143248	7.215665	p	0.0000	0.0000
NDVI	Mean	.2783816	.1176607	.1810828	t	31.9971	−24.0065
	Std. error	.0048309	.0017497	.0018252	p	0.0000	0.0000
NDBI	Mean	-.04239	.1864701	.1966282	t	−68.0658	−7.2790
	Std. error	.0048068	.0006194	.0010712	p	0.0000	0.0000
UI	Mean	-.3445721	.0613311	.0387379	t	−1.3e+02	11.7778
	Std. error	.0038092	.0008353	.0014767	p	0.0000	0.0000
VV	Mean	−10.5777	−3.182425	−5.190861	t	−95.5149	35.1953
	Std. error	.0707252	.0347708	.0406931	p	0.0000	0.0000

[a] Two-sample *t*-test.

risk of "class noise" (Nettleton et al., 2010) due to the existence of pixels of different classes within a polygon, which may bias the training and classification process. To reduce class noise, we perform an additional experiment using a dataset of 15,945 hand labeled examples (points), which we label as (1) "not built-up", (2) "built-up", (2a) "residential" and (2b) "non-residential"). We overlay the labeled points with the inputs (L8, SE1, SE2 and SE1SE2) and assign each pixel with a label according to the label of the overlapping point (each pixel is associated with exactly one point).

First, we examine the spectral characteristics (reflectance profile) of the examined classes, i.e., the average reflectance value of the pixels, per class and per band. Table 4 presents, as an example, the reflectance profile of the examined classes according to the spectral reflectance SE2. Consistent with built-up areas containing structures and impervious surfaces that are reflective relative to vegetation and undeveloped land of non-built-up areas, the reflectance of NBU pixels is lower than the reflectance of BU pixels in all bands. The difference in the reflectance of BU and NBU pixels is significant ($p = 0.000$) in all bands, and the standard error bounds of the average reflectance values are relatively small. The distinction between BU and NBU pixels is also expressed by a significantly higher NDVI value for NBU than for BU pixels, but by a significantly lower NDBI and UI value ($p < 0.01$ for both). As shown in Fig. 4, the distribution of the NDVI values of NBU regions is to the right of that of BU regions, while the distribution of the NDBI values of NBU pixels is a left-skewed and flatter than of BU pixels.

Moreover, we find differences between the spectral profile of residential and non-residential land use (Table 4). The reflectance is significantly different ($p < 0.05$) in all bands, besides B5 and B10, as well as in all spectral indices (NDVI, NDBI and UI). In addition, there is a significant difference ($P = 0.000$) between residential and non-residential land use in the reflectance of SE1`s C-band: the reflectance of residential land use is significantly ($p = 0.000$) higher than the reflectance of non-residential land use. Fig. 4 indicates that the distribution of SE1`s C-band of "residential" pixels is to the right of "non-residential" pixels, probably due to the existence of taller buildings and higher density which are associated with residential areas.

A 5-fold cross validation shows that the accuracy of the classification with the hand-labeled reference data (labeled points) is higher than classification with GDLA (labeled polygons) as the reference. This is indicated by a high balanced accuracy of 91% and 94% when classification is performed with L8 and SE1SE2 as inputs to the classifier, respectively (Table 5).

The accuracy of classification with the hand-labeled points exceeds the accuracy of classification with GDLA also for classification of residential and non-residential land use. The balanced accuracy ranges between 71% and 75% for classification with L8 and SE1SE2 as inputs to the classifiers, respectively (Table 5).

4.3. Mapping the classification

In the last stage of the classification, we use the classifiers that were trained with the hand-labeled examples to map the predicted class of each pixel. As clearly illustrated in Fig. 5, the classification captures the fabric of the built-up land cover and the fine boundaries between built-up and not built-up land cover. The difference between classification with L8 and SE1SE2 as inputs to the classifier is also illustrated when mapping the classifiers' predictions. Fig. 6 shows a comparison between classification with L8 and with SE1SE2 as inputs to the classifier. The figure illustrates that although classification with the two inputs captures the boundaries between built-up and not-built-up land cover, because of the higher spatial resolution of SE1SE2 compared to that of L8, classification with SE1SE2 captures individual structures with higher precision than classification with L8 as input to the classifier.

We also map the classifier's prediction of residential and non-residential land use. Fig. 7 presents, as an example, the classification of residential and non-residential land use (in this example, industrial areas), in the center of the city (classification with SE1SE2 as input). Note, that non-residential features appear in the satellite image as brighter (probably due to different types of structures and roofs) and less dense than residential features (Fig. 7).

4.4. Mapping urbanization across time

Finally, we map the built-up land cover across time. Because our hand-labeled examples are collected based on recent imagery, using this dataset as the reference for classification of historical imagery may result in "class-noise" due to mislabeled examples (e.g., a "built-up" pixel that was not "built-up" in a historical image). To cope with the lack of ground truth data for historic years, we train the classifier (using Random Forest, with 20 trees) with 2015 Landsat 7 as the input, and classify the built-up land cover in the historical imagery with the trained classifier (note, that we use the same feature space in the historical imagery). We find that in the period between 2000 and 2015, Ho Chi Minh City expanded from the city center primarily toward Northeast (Fig. 8). As illustrated in Fig. 9, while the city's central districts showed an increase of less than 10% in built-up land cover, its peripheral districts (the second and third rings) showed a more significant change (an increase of more than 70% in built-up land cover).

4.5. Built-up land cover as the distribution of the population

To understand the relation between the extent of built-up land cover and the distribution of the population in Ho Chi Minh City, we examine the correlation between the total area of built-up land cover in each district and two indicators: population counts (according to the 2015 Population and Labor Statistics[2]) and the intensity of the light emitted at night (according to DMSP-OLS and VIIRS). The results show a high and

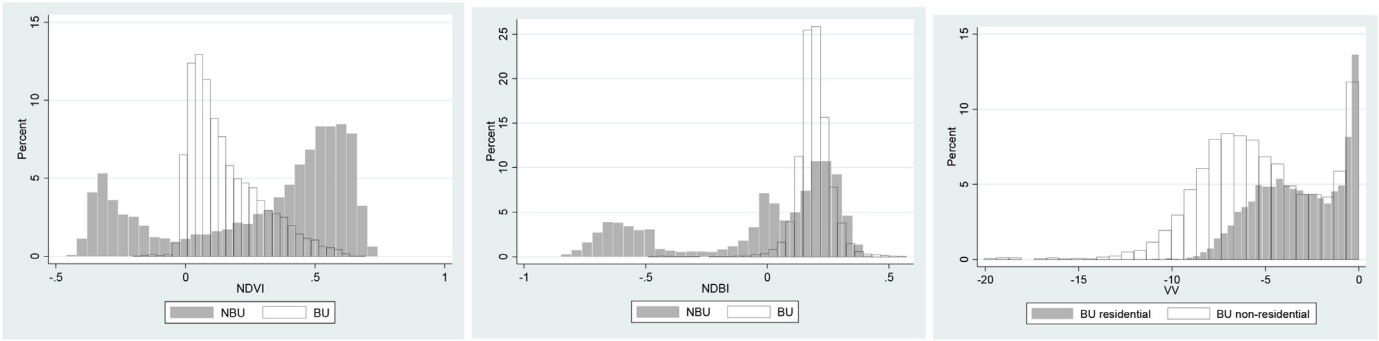

Fig. 4. The histogram of NDVI (Normalized Difference Vegetation Index) (left), NDBI (Normalized Difference Built-up Index) (middle) and SE1 C-Band (VV) (right) values, for built-up (BU), not built-up (NBU), built-up residential (BU residential) and built-up non-residential (BU non-residential) examples.

Table 5
Performance measures and confusion matrixes: classification of built-up vs. not built-up (top) and residential vs. non-residential pixels (bottom) (reference data: hand-labeled examples).

	L8				SE2				SE1				SE1SE2			
	built-up and not-built-up															
			predicted				predicted				predicted				predicted	
			BU	NBU			BU	NBU			BU	NBU			BU	NBU
	actual	BU	10256	574	actual	BU	10384	446	actual	BU	8932	1898	actual	BU	10468	362
		NBU	702	4411		NBU	536	4577		NBU	2256	2859		NBU	408	4703
Overall	92.0%				93.8%				73.9%				95.2%			
Producer's	94.7%				95.9%				82.5%				96.7%			
TNR	86.3%				89.5%				55.9%				92.0%			
Balanced	90.5%				92.7%				69.2%				94.3%			
User's	93.6%				95.1%				79.8%				96.2%			
	residential and non-residential															
			predicted				predicted				predicted				predicted	
			Res	NRes			Res	NRes			Res	NRes			Res	NRes
	actual	Res	5288	1157	actual	Res	5387	1058	actual	Res	4147	2298	actual	Res	5393	1052
		NRes	1717	2668		NRes	1662	2723		NRes	1980	2405		NRes	1466	2919
Overall	73.5%				74.9%				60.5%				76.7%			
TPR	82.0%				83.6%				64.3%				83.7%			
TNR	60.8%				62.1%				54.8%				66.6%			
Balanced	71.4%				72.8%				59.6%				75.1%			
Precision	75.5%				76.4%				67.7%				78.6%			

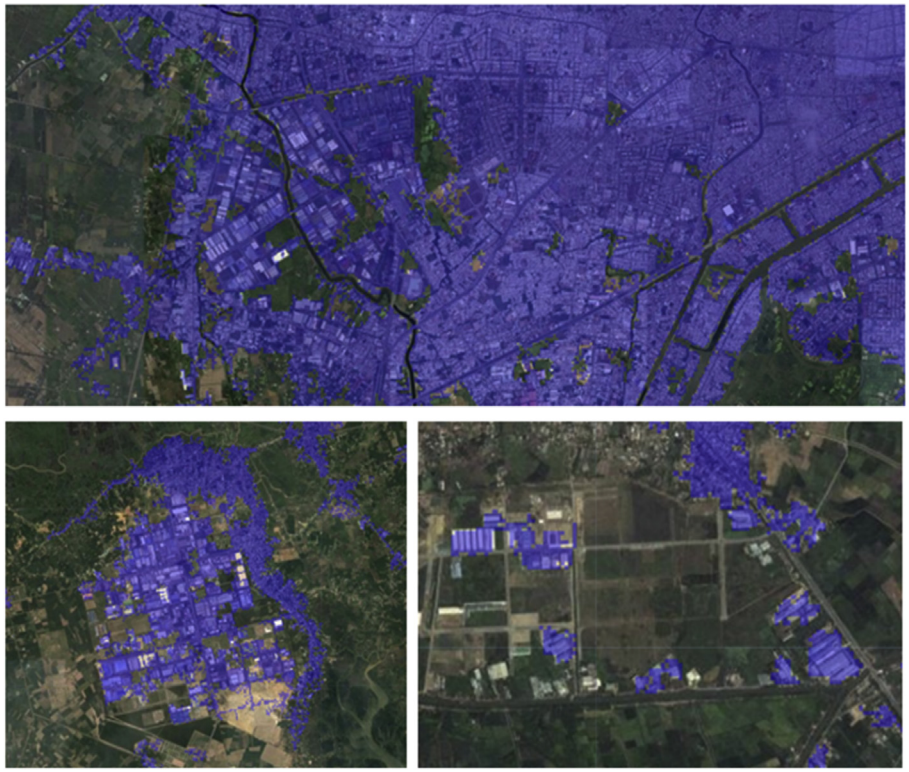

Fig. 5. Detection of built-up areas (in blue). Classification with SE1SE2.

significant correlation between total area of built-up land cover and population size (around $r = 0.93$, $p = 0.000$, with all inputs to the classifier) (Table 6 and Fig. 10). Additionally, we find a high and significant correlation ($p = 0.000$) between the total area of built-up land cover and the Sum of Light (SOL) measure. The correlation between DMSP-OLS SOL and built-up cover ranges between $r = 0.83$ and $r = 0.88$ for classificaiton with L8 and with SE1SE2, respectively. The correlation between VIIRS SOL and the area of built-up land cover is higher (around $r = 0.96$, $p = 0.000$, for classificaiton with all inputs to the classifier) (Table 6 and Fig. 11). These results indicate that the extent of built-up land cover is highly correlated with the distribution of the population, as measured according to population counts and according to the intensity of light emitted at night.

5. Discussion

Since the beginning of the 20th century, as the world's population has grown exponentially from around 1.6 billion in 1900 to around 7.6

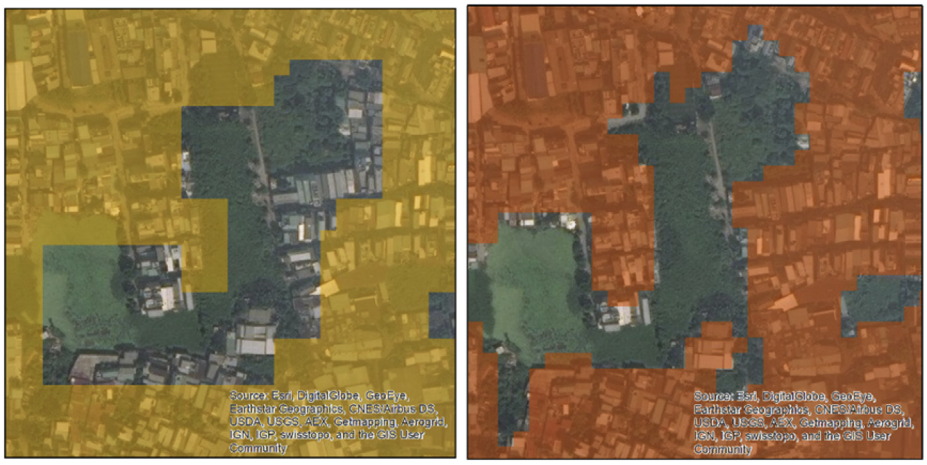

Fig. 6. Classification of built-up land cover with L8 (left) and with SE1SE2 (right) as input to the classifier.

billion today, the global urban population has grown equally dramatically from 220 million in 1900 to 3.9 billion in 2014. By 2050, 66 per cent of the global population is expected to be urban, with nearly 90 per cent of the increase concentrated in Asia and Africa (UN, 2014, 2006).

While urbanization in rapidly growing nations is helping lift hundreds of millions of people out of poverty, it also creates immense societal challenges by increasing greenhouse-gas emissions, destabilizing fragile ecosystems, and creating new demands on public services and infrastructure that impose significant burdens on the environment (Ban et al., 2015). The rapid expansion of built environments is among the most irreversible human impacts on the global biosphere (Zhang and Seto, 2011).

Traditionally, data on urbanization has come from census counts and population surveys, which are often published infrequently, vary in terms of their resolution and precision, and are subject to the availability of resources and the capacity to acquire reliable data (Keola et al., 2015), and to local and national definitions of urbanization (Montgomery, 2008). Significant progress in the availability of remotely sensed data and machine learning have substantially improved our understanding about the extent and pace of urbanization. However, developing classification procedures that are robust and repeatable across space and time is challenging (Franklin and Wulder, 2002; Ma et al., 2017) and the majority of studies that utilize remotely sensed data for urban research have focused on local or regional scales. Although multiple classification schemes have been developed to map global urbanization (Bartholomé and Belward, 2005, p. 200; de Colstoun et al., 2017; Esch et al., 2017; Pesaresi et al., 2013), they typically map urbanization in specific points in time and according to a specific definition of 'urban'. Until recently, researchers have been limited to the availability and of these products.

Emerging cloud based computational platforms such as Google Earth Engine (GEE) now provide handy and easy-to-use tools to extract information from remotely sensed data. GEE is a cloud-based platform "*that makes it easy to access high-performance computing resources for processing very large geospatial datasets, without having to suffer the IT pains currently surrounding either*" (Gorelick et al., 2017). Users can now use publicly available satellite imagery together with any available source of location-specific reference data to map LC/LU at any location on Earth and in any point in time.

In this study, we demonstrate the applicability of GEE to map built-up LC/LU in one province in Vietnam – Ho Chi Minh City (HCMC). We perform pixel-based supervised image classification using three sources of publicly available data: Landsat 8, Sentinel-1 and Sentine-2, together with administrative cadastral data (GDLA) and a dataset of around 16,000 hand-labeled examples as reference. We show that basic off-the-shelf supervised image classification techniques can be used to accurately map annual changes in the extent built-up land cover in the province and to differentiate between residential and non-residential land use.

The success of mapping complex heterogeneous urban settings largely depends on the spatial and spectral characteristics of the remotely sensed data used for classification (Herold et al., 2002; Momeni et al., 2016; Oltra-Carrió et al., 2015; Pesaresi et al., 2016a; Rashed and Jürgens, 2010; Small, 2016). Fusing data collected by multiple sources allows one to capture the characteristics of land cover on Earth and thereby improve the accuracy of the classification (Amarsaikhan et al., 2007; Joshi et al., 2016; Pesaresi et al., 2016a; Wang et al., 2017). Here, we show that pixel based image classification based on publicly available satellite imagery results in accurate maps of built-up LC/LU in HCMC. As expected, classification with Sentinel-2 (SE2) as input to the classifier exceeds the accuracy of classification with Ladsat-8 (L8) by up to 2.2%, which we relate to the spatial and spectral resolution of SE2 compared to L8.

Sentinel-1 (SE1) provides C-Band SAR data, which is useful in characterizing highly dense urban settings. Nevertheless, SAR data is inherently affected by speckle noise, which is caused by the presence of randomly distributed elemental scatterers within a resolution cell (Moreira et al., 2013). As a result, SAR response may be more related to scatterer density than to the actual characteristics of the surface, especially in high-density urban areas (Dell'Acqua and Gamba, 2003). Here, we show that fusing moderate-resolution optical and radar data (SE2 and SE1, respectively) increases the accuracy of the classification (indicated by a balanced accuracy rate of up to 94%). As pointed out by (Amarsaikhan et al., 2010), urban areas are complex and diverse in nature, and many features have similar spectral characteristics, making it difficult to differentiate among them. The added value of the radar data (SE1) is its sensitivity to the geometry, texture and density of the surface. We note that using SAR data at a finer spatial resolution than SE1 may not be sufficient for pixel-based classification, especially in dense and vertically heterogeneous urban settings, because the speckle may cause the SAR returns to be placed in different pixels than the optical reflectance returns.

Classification accuracy of remotely sensed data is also affected by the quality of the reference data and their "noise" (Foody et al., 2016; Pelletier et al., 2017), as well as by the number of training examples, their collection strategy and their representativeness of the landscapes (Lu and Weng, 2007). Although the Vietnamese Government, through GDLA, had routinely allocated vast amounts of resources to generate land use maps at 5-yearly intervals, our results show that with the hand-labeled examples as reference to the classifier, classification improves compared to classification with GDLA. This is because our hand labeled examples (points) characterize the LC/LU in an exact location compared to GDLA, where the LC/LU is characterized as continuous homogenous polygons where pixels are aggregated into uniform areas. This difference in classification accuracy can also be viewed in light of the Modifiable Areal

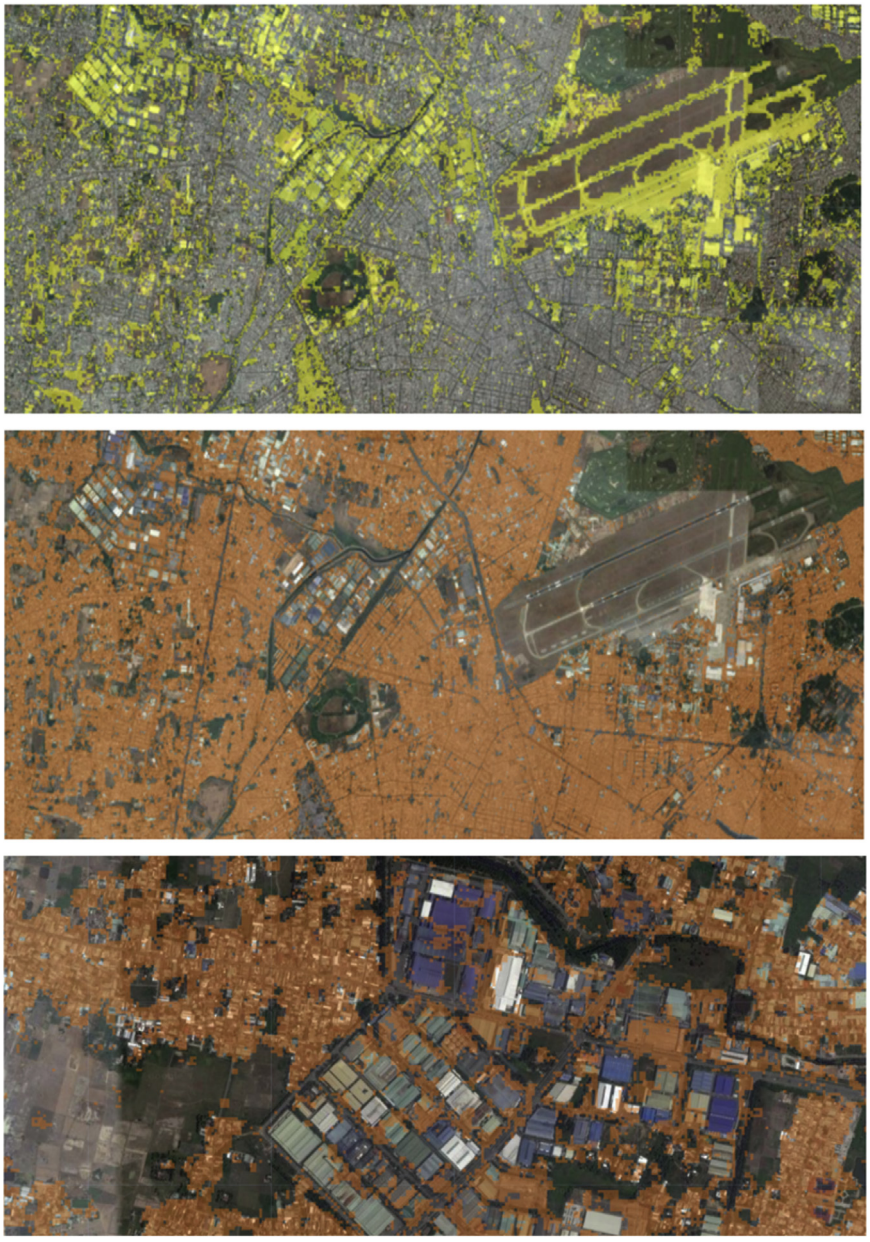

Fig. 7. Classification of residential (yellow) and non-residential (orange) land use.

Unit Problem (MAUP) (Openshaw and Openshaw, 1984), which arises "*from the imposition of artificial units of spatial reporting on continuous geographical phenomena resulting in the generation of artificial spatial patterns*" (Heywood et al., 1998). Here, the smallest units of analysis are pixels, arbitrary in size, that typically do not correspond well with real-world objects (Johnson and Xie, 2013). Pixels can be aggregated to form larger polygons, which may vary in scale (known as the scale effect) or in shape, or form (known as the zoning effect) (Fotheringham and Rogerson, 2008; Jelinski and Wu, 1996). Different aggregation procedures and definitions may cause variation in the analyzed data, and in turn, in the derived conclusions (Jelinski and Wu, 1996). While our results using GDLA inherently depend on the scale and form of this specific data and use of other types of aggregation may generate different results, they clearly suggest that a revision of the Government's procedures for data acquisition could not only generate cost savings but also enhance the quality and frequency of available information and thus may allow new types of applications to be developed.

Previous studies that utilize remotely sensed data have focused on mapping the characteristics of Earth's *land cover* (Pesaresi et al., 2016a; Su et al., 2015; Zhang et al., 2002). While *land cover* denotes the physical and biotic character of the land surface, *land use* denotes the human employment of the land (Meyer and B. L. Turner, 1992). Only a limited number of studies have explored the use of remotely sensed data for classification of land use in urban settings (e.g. Hu et al., 2016). In this study, we show that publicly available remotely sensed data can be used to differentiate between residential and non-residential built-up land use. Although classification of land use with GDLA as reference does not result in highly accurate maps (a balanced accuracy of 68% with SE1SE2 as input to the classifier), accuracy improves with the hand-labeled examples as reference (indicated by a balanced accuracy of 75% with SE1SE2). The addition of SE1 to SE2 as input to the classifier improves the accuracy of the classification by up to 2.3%.

Finally, we use our hand-labeled examples as reference to train a classifier with Landsat-7 2015 data as input and map historic changes in built-up land cover. We find that between 2000 and 2015, as HCMC has expanded dramatically, some districts show more than 70% increase in

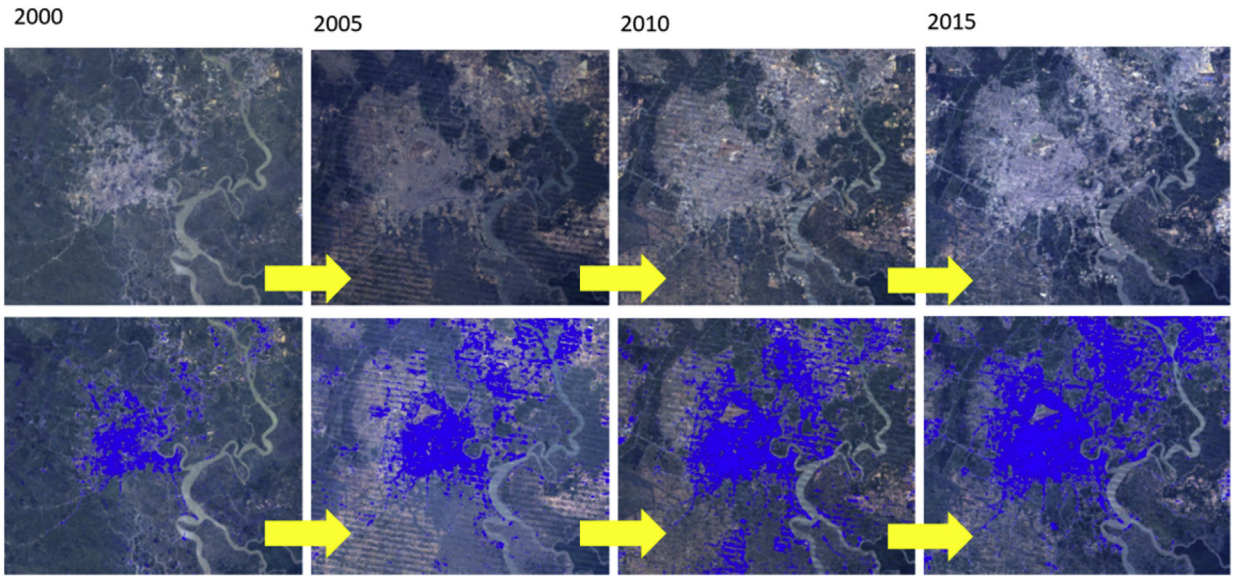

Fig. 8. Annual changes in the extent of built-up land cover, Ho Chi Minh City (top: reference image (Landsat); bottom: classification of built-up land cover (in blue)).

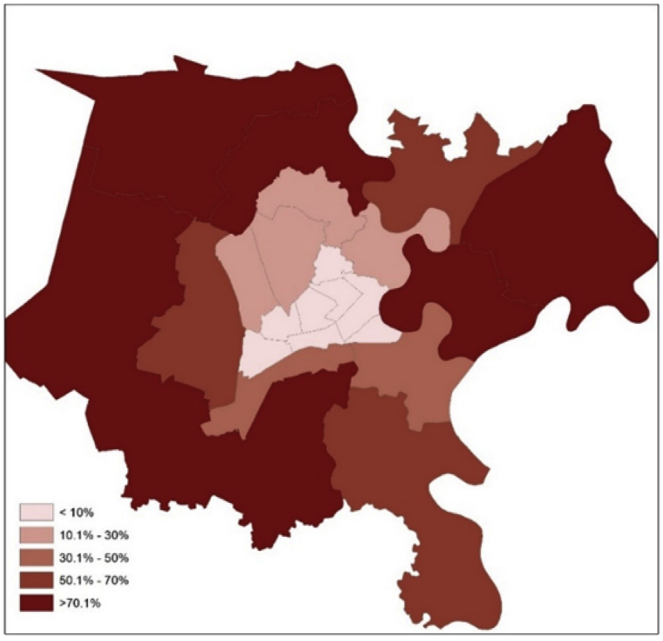

Fig. 9. Percent of change in built-up land cover, per district (Ho Chi Minh city).

Table 6
Correlations between the total area of built-up land cover, total population and SOL (according to DMSP-OLS and VIIRS), per district.

		Total areas classified as "built-up"		
		L8	SE2	SE2SE1
VIIRS	r	0.9609	0.9670	0.9674
	p	0.000	0.0000	0.0000
	R^2	0.923	0.935	0.936
DMSP-OLS	r	0.8283	0.8803	0.8784
	p	0.0000	0.0000	0.0000
	R^2	0.686	0.775	0.772
2015 Population count	r	0.9369	0.9261	0.9270
	p	0.0000	0.0000	0.0000
	R^2	0.878	0.858	0.859

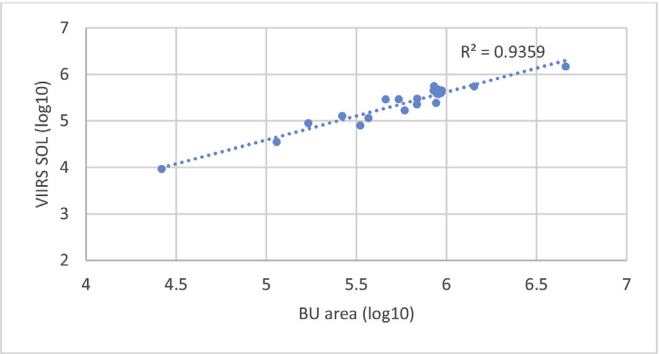

Fig. 10. Correlation between total built-up land cover and SOL (VIIRS).

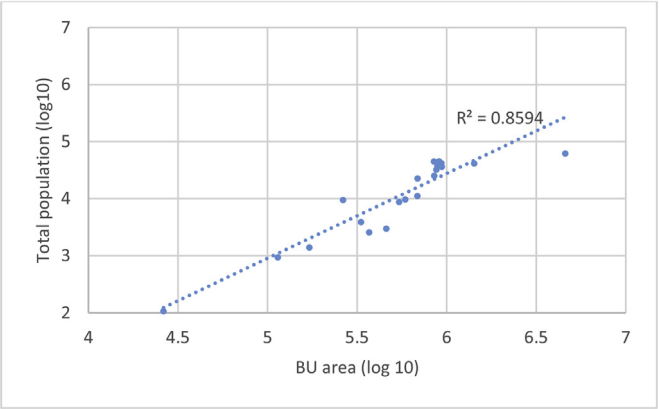

Fig. 11. Correlation between total built-up land cover and population size (per district).

the built-up land cover in the city's peripheral districts. According to Kontgis et al. (2014), between 1990 and 2000, the city's urban expansion was almost exclusively contiguous to urban core communes, while between 2000 and 2012, new urban land became patchier and disconnected from urban core communes. Between 1992 and 2012, approximately one-third of new urban expansion occurred in locations distant more than 40 km from the core. These trends are due, in part, to

significant development in Ho Chi Minh City's periphery in the first decade of 2000. To illustrate, between 2006 and 2009 the city's peripheral and rural areas have been the site of 36 housing projects that convert farming to urban land compared to only 19 projects being built in the core areas and inner-city districts (Hirsch, 2016).

In parallel to the expansion of the built-up land cover, Ho Chi Minh City experienced rapid population growth, especially in its peri-urban and rural districts (Downes et al., 2016). Many studies suggest a close relationship between the distribution of built-up land cover and the distribution of the population in a city (Bagan and Yamagata, 2015; Sudhira et al., 2004; Yin et al., 2005), also as it is measured according to the intensity of light emitted at night (Huang et al., 2014). The results of this study show a high and significant correlation between the distribution of the built-up land cover in Ho Chi Minh City and the distribution of its population, both, according to population counts and the intensity of nighttime light. We find, however, a higher correlation between the distribution of built-up land cover and nighttime light (SOL) as measured by VIIRS than by DMSP-OLS. This finding is consistent with previous studies that show that nighttime light data extracted from VIIRS represents more accurately the distribution of built-up urban areas and the distribution of the population than nighttime light data extracted from DMSP-OLS (Chen and Nordhaus, 2015; K. Shi et al., 2014a).

This paper contributes to the existing literature in several aspects. First, it demonstrates the applicability of publicly available satellite data for mapping LC/LU with high precision and importantly, at any point in time. Today, researchers and decision makers no longer need to rely on classification products that were created for specific locations, specific points in time or according to a specific definition. As we show, with basic off-the-shelf supervised image classification algorithms, publicly available datasets and cloud based computation platforms, extraction of meaningful information about Earth across space and time becomes easier and more accessible. Second, a key challenge in any supervised machine learning is the lack of reference data. We show that existing administrative cadastral data can be used as reference for classification of LC/LU across time. Moreover, with modest effort, hand-labeled examples can be collected and used as reference to improve the accuracy of the classification. Third, we perform a systematic comparison between three types of publicly available remotely sensed data as inputs for classification (L8, SE1 and SE2) and show the added value of fusing SE1 and SE2 for classification of an urban settings. The study demonstrates that using SE1 and SE2 combined as input for classification results in highly accurate maps of urbanization. Finally, remote sensing studies have traditionally focused on mapping land cover rather than land use. This is because different types of land use are often characterized by similar spectral reflectance. Here, we show that supervised pixel-based image classification can also be utilized to differentiate between two types of built-up land use in an urban environment: residential and non-residential. This distinction is important, for example, for taxation purposes or for population estimation.

We note three limitation of the study, which merit attention. First, reference databases are theoretically and ideally, a gold-standard, that provides the "correct" label for each referenced instance. However, in practice, reference data are often "noisy". Class label noise may occur during data collection or field surveys due to a lack of information, the subjectivity of human judgment, or human mistakes (Pelletier et al., 2017). We collected our hand-labeled examples through image interpretation technique performed by graduate students. Idiosyncratic variation across individuals performing the manual classification is often difficult to control and may affect the "noise" in the data (Congalton and Green, 2008) and the reported accuracy of the classification. In addition, we performed pixel-based classification with a basic Random Forest classifier. As noted in previous studies, performance of Random Forests is subject to many parameters, such as the number of examples used for training (Foody, 2002; Rodriguez-Galiano et al., 2012), the class proportion (Rodriguez-Galiano et al., 2012), the spatial distribution of the examples (Millard and Richardson, 2015), the number of trees in the forest (Zhang et al., 2012) and the input feature space (Goldblatt et al., 2016). However, other studies suggest that the setting of Random Forest parameters causes little influence on the classification accuracy (Pelletier et al., 2016). In addition, the RF classifier achieves better classification results when multi-dimensional data such as hyperspectral or multi-source data are used; it also requires the setting of fewer parameters (Belgiu and Drăguţ, 2016).

Second, in this study we mapped the built-up land cover in one province in Vietnam, using reference data collected for one specific region. These results do not imply the spatial generalization of the model. Although classification performance often decreases when the landscapes characteristics are different from those of the training area (Pelletier et al., 2016), Random forest classifiers can also be generalized spatially and applied across space and time (Goldblatt et al., 2016). The confusion matrix and the accuracy estimates derived from it provide no information on the spatial distribution of error (Foody, 2005), and the results we report here only describe a location specific classification accuracy (within-image accuracy).

Third, we performed pixel-based classification with a Random Forest classifier. Random Forests are often seen as "black boxes" consisting of multiple decision trees, and it is hard to examine the individual trees separately (Prasad et al., 2006). We did not aim here to develop a new classifier or to improve an existing one. Nor did we aim to perform in-depth examination of the decision trees and splits in the forests. Our objective was to highlight the use of off-the-shelf classifiers and input data for LC/LU classification.

To summarize, in this study we illustrated the applicability of publicly available satellite data for accurately mapping the built-up land cover and land use in one province in Vietnam. While many existing classification products characterize urbanization, they are typically limited in their spatial and temporal resolution and characterize urbanization according to definitions that may have limited application in other contexts. Existing products often do not allow continuous monitoring of urbanization processes. Cloud-based computation platforms, such as GEE, now provide an easy solution for LC/LU mapping using publicly available data and geographically specific reference data. In today's era of big data, a tractable method of defining and classifying built-up areas has extensive application. Economics, urban planning, climate modeling, water-resource management, hazard-response efforts, and urban-ecosystem assessments all use geographic data on urban areas. With earth's rapidly urbanizing population, having information on urban extent that is spatially and temporally consistent and defined at high resolution is both relevant to a wide range of disciplines and essential for helping society better understand the drivers of urbanization.

References

Abdikan, S., Sanli, F.B., Sunar, F., Ehlers, M., 2014. A comparative data-fusion analysis of multi-sensor satellite images. Int. J. Digit. Earth 7, 671–687. https://doi.org/10.1080/17538947.2012.748846.

Amarsaikhan, D., Ganzorig, M., Ache, P., Blotevogel, H., 2007. The integrated use of optical and InSAR data for urban land-cover mapping. Int. J. Remote Sens. 28, 1161–1171. https://doi.org/10.1080/01431160600784267.

Amarsaikhan, D., Blotevogel, H.H., Genderen, J.L., van Ganzorig, M., Gantuya, R., Nergui, B., 2010. Fusing high-resolution SAR and optical imagery for improved urban land cover study and classification. Int. J. Image Data Fusion 1, 83–97. https://doi.org/10.1080/19479830903562041.

Archer, K., Bezdecny, K., 2016. Handbook of Cities and the Environment. Edward Elgar Publishing.

Arlot, S., Celisse, A., 2010. A survey of cross-validation procedures for model selection. Stat. Surv. 4, 40–79. https://doi.org/10.1214/09-SS054.

Arouri, M., Ben Youssef, A., Nguyen, C., 2017. Does urbanization reduce rural poverty? Evidence from Vietnam. Econ. Modell. 60, 253–270. https://doi.org/10.1016/j.econmod.2016.09.022.

Bagan, H., Yamagata, Y., 2015. Analysis of urban growth and estimating population density using satellite images of nighttime lights and land-use and population data. GIScience Remote Sens. 52, 765–780. https://doi.org/10.1080/15481603.2015.1072400.

Ban, Y., Jacob, A., Gamba, P., 2015. Spaceborne SAR data for global urban mapping at 30m resolution using a robust urban extractor. ISPRS J. Photogramm. Remote Sens. Global Land Cover Mapp. Monit. 103, 28–37. https://doi.org/10.1016/j.isprsjprs.2014.08.004.

Bartholomé, E., Belward, A.S., 2005. GLC2000: a new approach to global land cover mapping from Earth observation data. Int. J. Remote Sens. 26, 1959–1977. https://doi.org/10.1080/01431160412331291297.
Baum-Snow, N., 2007. Did highways cause suburbanization? Q. J. Econ. 122, 775–805. https://doi.org/10.1162/qjec.122.2.775.
Béland, M., Goïta, K., Bonn, F., Pham, T.T.H., 2006. Assessment of land-cover changes related to shrimp aquaculture using remote sensing data: a case study in the Giao Thuy District, Vietnam. Int. J. Remote Sens. 27, 1491–1510. https://doi.org/10.1080/01431160500406888.
Belgiu, M., Drăguţ, L., 2016. Random forest in remote sensing: a review of applications and future directions. ISPRS J. Photogrammetry Remote Sens. 114, 24–31. https://doi.org/10.1016/j.isprsjprs.2016.01.011.
Belgiu, M., Drăguţ, L., 2014. Comparing supervised and unsupervised multiresolution segmentation approaches for extracting buildings from very high resolution imagery. ISPRS J. Photogramm. Remote Sens. 96, 67–75. https://doi.org/10.1016/j.isprsjprs.2014.07.002.
Bhatta, B., 2009. Analysis of urban growth pattern using remote sensing and GIS: a case study of Kolkata, India. Int. J. Remote Sens. 30, 4733–4746. https://doi.org/10.1080/01431160802651967.
Blum, A., Kalai, A., Langford, J., 1999. Beating the hold-out: Bounds for K-fold and progressive cross-validation. In: Proceedings of the Twelfth Annual Conference on Computational Learning Theory, COLT '99. ACM, New York, NY, USA, pp. 203–208. https://doi.org/10.1145/307400.307439.
Bojo, J., 2011. Vietnam Development Report 2011: Natural Resources Management (No. 66634). The World Bank.
Bradford, J.P., Brodley, C.E., 2001. The effect of instance-space partition on significance. Mach. Learn. 42, 269–286. https://doi.org/10.1023/A:1007613918580.
Castella, J.-C., Pheng Kam, S., Dinh Quang, D., Verburg, P.H., Thai Hoanh, C., 2007. Combining top-down and bottom-up modelling approaches of land use/cover change to support public policies: application to sustainable management of natural resources in northern Vietnam. Land Use Policy Integr. Assess. Land Syst.: Future Land Use 24, 531–545. https://doi.org/10.1016/j.landusepol.2005.09.009.
Chen, X., Nordhaus, W., 2015. A test of the new VIIRS lights data set: population and economic output in Africa. Rem. Sens. 7, 4937–4947. https://doi.org/10.3390/rs70404937.
Chen, Jun, Chen, Jin, Liao, A., Cao, X., Chen, L., Chen, X., He, C., Han, G., Peng, S., Lu, M., Zhang, W., Tong, X., Mills, J., 2015. Global land cover mapping at 30 m resolution: a POK-based operational approach. ISPRS J. Photogramm. Remote Sens. Global Land Cover Mapp. Monit. 103, 7–27. https://doi.org/10.1016/j.isprsjprs.2014.09.002.
Chen, D., Stow, D.A., Gong, P., 2004. Examining the effect of spatial resolution and texture window size on classification accuracy: an urban environment case. Int. J. Remote Sens. 25, 2177–2192. https://doi.org/10.1080/01431160310001618464.
Chen, Z., Zhang, Y., Guindon, B., Esch, T., Roth, A., Shang, J., 2013. Urban land use mapping using high resolution SAR data based on density analysis and contextual information. Can. J. Remote Sens. 38, 738–749. https://doi.org/10.5589/m13-002.
CIESIN, 2005. Gridded Population of the World (GPWv3) Data Collection, Version 3.
Cohen, B., 2006. Urbanization in developing countries: current trends, future projections, and key challenges for sustainability. Technol. Soc. 28, 63–80. https://doi.org/10.1016/j.techsoc.2005.10.005.
Congalton, R.G., Green, K., 2008. Assessing the Accuracy of Remotely Sensed Data: Principles and Practices, Second ed. CRC Press.
Dasgupta, S., Deichmann, U., Meisner, C., Wheeler, D., 2005. Where is the poverty–environment Nexus? Evidence from Cambodia, Lao PDR, and Vietnam. World Dev. 33, 617–638. https://doi.org/10.1016/j.worlddev.2004.10.003.
de Colstoun, E.C.B., Huang, C., Wang, P., Tilton, J.C., Tan, B., Phillips, J., Niemczura, S., Ling, P.-Y., Wolfe, R., 2017. Documentation for the Global Man-made Impervious Surface (GMIS) Dataset from Landsat.
Decision No. 445/QD-TTg, 2009. Decision No. 445/QD-ttg Dated April 17th 2009, Approving Modification of the Master Plan for Development of Vietnam's Urban System by 2025 with Vision to 2050 [WWW Document]. http://hethongphapluatvietnam.net/decision-no-445-qd-ttg-dated-april-17th-2009-approving-modification-of-the-master-plan-for-development-of-vietnam-s-urban-system-by-2025-with-vision-to-2050.html. (Accessed 18 January 2018).
Dell'Acqua, F., Gamba, P., 2003. Texture-based characterization of urban environments on satellite SAR images. IEEE Trans. Geosci. Rem. Sens. 41, 153–159. https://doi.org/10.1109/TGRS.2002.807754.
Dewan, A.M., Yamaguchi, Y., 2009. Land use and land cover change in Greater Dhaka, Bangladesh: using remote sensing to promote sustainable urbanization. Appl. Geogr. 29, 390–401. https://doi.org/10.1016/j.apgeog.2008.12.005.
Downes, N.K., Storch, H., Schmidt, M., Nguyen, T.C.V., Dinh, L.C., Tran, T.N., Hoa, L.T., 2016. Understanding Ho Chi Minh City's urban structures for urban land-use monitoring and risk-adapted land-use planning. In: Sustainable Ho Chi Minh City: Climate Policies for Emerging Mega Cities. Springer, Cham, pp. 89–116. https://doi.org/10.1007/978-3-319-04615-0_6.
Elvidge, C.D., Baugh, K.E., Zhizhin, M., Hsu, F.-C., 2013. Why VIIRS data are superior to DMSP for mapping nighttime lights. Proc. Asia Pac. Adv. Netw. 35, 62–69.
Elvidge, C., Hsu, F.-C., Baugh, K., Ghosh, T., 2014. National trends in satellite-observed lighting: 1992-2012. In: Global Urban Monitoring and Assessment through Earth Observation, Remote Sensing Applications Series. CRC Press, pp. 97–120.
Elvidge, C.D., Baugh, K., Zhizhin, M., Hsu, F.C., Ghosh, T., 2017. VIIRS night-time lights. Int. J. Remote Sens. 0, 1–20. https://doi.org/10.1080/01431161.2017.1342050.
Esch, T., Heldens, W., Hirne, A., Keil, M., Marconcini, M., Roth, A., Zeidler, J., Dech, S., Strano, E., 2017. Breaking New Ground in Mapping Human Settlements from Space -The Global Urban Footprint. ArXiv170604862 Phys.
Estima, J., Painho, M., 2015. Investigating the potential of OpenStreetMap for land use/land cover production: a case study for continental Portugal. In: Arsanjani, J.J., Zipf, A., Mooney, P., Helbich, M. (Eds.), OpenStreetMap in GIScience, Lecture Notes in Geoinformation and Cartography. Springer International Publishing, pp. 273–293. https://doi.org/10.1007/978-3-319-14280-7_14.
Feyisa, G.L., Dons, K., Meilby, H., 2014. Efficiency of parks in mitigating urban heat island effect: an example from Addis Ababa. Landsc. Urban Plann. 123, 87–95. https://doi.org/10.1016/j.landurbplan.2013.12.008.
Flood, N., 2013. Seasonal composite Landsat TM/ETM+ images using the medoid (a multi-dimensional median). Rem. Sens. 5, 6481–6500. https://doi.org/10.3390/rs5126481.
Fonteh, M.L., Theophile, F., Cornelius, M.L., Main, R., Ramoelo, A., Cho, M.A., 2016. Assessing the utility of Sentinel-1 C band synthetic aperture radar imagery for land use land cover classification in a tropical coastal systems when compared with Landsat 8. J. Geogr. Inf. Syst. 08 (495) https://doi.org/10.4236/jgis.2016.84041.
Foody, G.M., 2002. Status of land cover classification accuracy assessment. Remote Sens. Environ. 80, 185–201. https://doi.org/10.1016/S0034-4257(01)00295-4.
Foody, G.M., 2005. Local characterization of thematic classification accuracy through spatially constrained confusion matrices. Int. J. Remote Sens. 26, 1217–1228. https://doi.org/10.1080/01431160512331326521.
Foody, G.M., Pal, M., Rocchini, D., Garzon-Lopez, C.X., Bastin, L., 2016. The sensitivity of mapping methods to reference data quality: training supervised image classifications with imperfect reference data. ISPRS Int. J. Geo-Inf. 5 (199) https://doi.org/10.3390/ijgi5110199.
Forkuor, G., Dimobe, K., Serme, I., Tondoh, J.E., 2017. Landsat-8 vs. Sentinel-2: examining the added value of sentinel-2's red-edge bands to land-use and land-cover mapping in Burkina Faso. GIScience Remote Sens. 0, 1–24. https://doi.org/10.1080/15481603.2017.1370169.
Fotheringham, A.S., Rogerson, P.A., 2008. The SAGE Handbook of Spatial Analysis. SAGE.
Franklin, S.E., Wulder, M.A., 2002. Remote sensing methods in medium spatial resolution satellite data land cover classification of large areas. Prog. Phys. Geogr. Earth Environ. 26, 173–205. https://doi.org/10.1191/0309133302pp332ra.
Gamba, P., 2014. Image and data fusion in remote sensing of urban areas: status issues and research trends. Int. J. Image Data Fusion 5, 2–12. https://doi.org/10.1080/19479832.2013.848477.
Gaughan, A.E., Stevens, F.R., Linard, C., Jia, P., Tatem, A.J., 2013. High resolution population distribution maps for Southeast Asia in 2010 and 2015. PLoS One 8, e55882. https://doi.org/10.1371/journal.pone.0055882.
Gislason, P.O., Benediktsson, J.A., Sveinsson, J.R., 2006. Random Forests for land cover classification. Pattern Recognit. Lett. 27, 294–300. https://doi.org/10.1016/j.patrec.2005.08.011. Pattern Recognition in Remote Sensing (PRRS 2004).
Goldblatt, R., You, W., Hanson, G., Khandelwal, A.K., 2016. Detecting the boundaries of urban areas in India: a dataset for pixel-based image classification in Google Earth Engine. Rem. Sens. 8 (634) https://doi.org/10.3390/rs8080634.
Goldblatt, R., Stuhlmacher, M.F., Tellman, B., Clinton, N., Hanson, G., Georgescu, M., Wang, C., Serrano-Candela, F., Khandelwal, A.K., Cheng, W.-H., Balling, R.C., 2018. Using Landsat and nighttime lights for supervised pixel-based image classification of urban land cover. Remote Sens. Environ. 205, 253–275. https://doi.org/10.1016/j.rse.2017.11.026.
Goodman, I.R., Mahler, R.P., Nguyen, H.T., 2013. Mathematics of Data Fusion. Springer Science & Business Media.
Gorelick, N., Hancher, M., Dixon, M., Ilyushchenko, S., Thau, D., Moore, R., 2017. Google Earth Engine: Planetary-scale geospatial analysis for everyone. Remote Sens. Environ. Big Remotely Sens. Data Tools Appl. Exp. 202, 18–27. https://doi.org/10.1016/j.rse.2017.06.031.
Guan, H., Li, J., Chapman, M., Deng, F., Ji, Z., Yang, X., 2013. Integration of orthoimagery and lidar data for object-based urban thematic mapping using random forests. Int. J. Rem. Sens. 34, 5166–5186. https://doi.org/10.1080/01431161.2013.788261.
Haack, B., D Herold, N., A Bechdol, M., 2000. Radar and Optical Data Integration for Land-Use/Land-cover Mapping.
Henderson, V., 2002. Urbanization in developing countries. World Bank Res. Obs. 17, 89–112.
Henderson, M., Yeh, E.T., Gong, P., Elvidge, C., Baugh, K., 2003. Validation of urban boundaries derived from global night-time satellite imagery. Int. J. Remote Sens. 24, 595–609. https://doi.org/10.1080/01431160304982.
Henderson, J.V., Storeygard, A., Weil, D.N., 2012. Measuring economic growth from outer space. Am. Econ. Rev. 102, 994–1028. https://doi.org/10.1257/aer.102.2.994.
Herold, M., 2009. Some recommendations for global efforts in urban monitoring and assessments from remote sensing. In: Global Mapping of Human Settlement, Remote Sensing Applications Series. CRC Press. https://doi.org/10.1201/9781420083408-c2.
Herold, M., Gardner, M., Hadley, B., Roberts, D., 2002. The spectral dimension in urban land cover mapping from high-resolution optical remote sensing data. In: Proceedings of the 3 rd Symposium on Remote Sensing of Urban Areas.
Herold, M., Gardner, M.E., Roberts, D.A., 2003. Spectral resolution requirements for mapping urban areas. IEEE Trans. Geosci. Rem. Sens. 41, 1907–1919. https://doi.org/10.1109/TGRS.2003.815238.
Heywood, I., Cornelius, S., Carver, S., 1998. An Introduction to Geographical Information Systems. Addison Wesley Longman, Harlow.
Hirsch, P., 2016. Routledge Handbook of the Environment in Southeast Asia. Taylor & Francis.
Hu, X., Li, Y., Shan, J., Zhang, J., Zhang, Y., 2014. Road centerline extraction in complex urban scenes from LiDAR data based on multiple features. IEEE Trans. Geosci. Rem. Sens. 52, 7448–7456. https://doi.org/10.1109/TGRS.2014.2312793.
Hu, T., Yang, J., Li, X., Gong, P., 2016. Mapping urban land use by using Landsat images and open social data. Rem. Sens. 8 (151) https://doi.org/10.3390/rs8020151.

Huang, Q., Yang, X., Gao, B., Yang, Y., Zhao, Y., 2014. Application of DMSP/OLS nighttime light images: a meta-analysis and a systematic literature review. Rem. Sens. 6, 6844–6866. https://doi.org/10.3390/rs6086844.
Jat, M.K., Garg, P.K., Khare, D., 2008. Monitoring and modelling of urban sprawl using remote sensing and GIS techniques. Int. J. Appl. Earth Obs. Geoinf. 10, 26–43. https://doi.org/10.1016/j.jag.2007.04.002.
Jean, N., Burke, M., Xie, M., Davis, W.M., Lobell, D.B., Ermon, S., 2016. Combining satellite imagery and machine learning to predict poverty. Science 353, 790–794. https://doi.org/10.1126/science.aaf7894.
Jelinski, D.E., Wu, J., 1996. The modifiable areal unit problem and implications for landscape ecology. Landsc. Ecol. 11, 129–140. https://doi.org/10.1007/BF02447512.
Jiang, Z., Huete, A.R., Didan, K., Miura, T., 2008. Development of a two-band enhanced vegetation index without a blue band. Remote Sens. Environ. 112, 3833–3845. https://doi.org/10.1016/j.rse.2008.06.006.
Johnson, B., Xie, Z., 2013. Classifying a high resolution image of an urban area using super-object information. ISPRS J. Photogramm. Remote Sens. 83, 40–49. https://doi.org/10.1016/j.isprsjprs.2013.05.008.
Joshi, N., Baumann, M., Ehammer, A., Fensholt, R., Grogan, K., Hostert, P., Jepsen, M.R., Kuemmerle, T., Meyfroidt, P., Mitchard, E.T.A., Reiche, J., Ryan, C.M., Waske, B., 2016. A review of the application of optical and radar remote sensing data fusion to land use mapping and monitoring. Rem. Sens. 8 (70) https://doi.org/10.3390/rs8010070.
Kawamura, M., Jayamana, S., Tsujiko, Y., 1996. Relation between social and environmental conditions in Colombo Sri Lanka and the urban index estimated by satellite remote sensing data. Int. Arch. Photogramm. Remote Sens. 31, 321–326.
Keola, S., Andersson, M., Hall, O., 2015. Monitoring economic development from space: using nighttime light and land cover data to measure economic growth. World Dev. 66, 322–334. https://doi.org/10.1016/j.worlddev.2014.08.017.
Kii, M., Nakamura, K., 2017. Development of a suitability model for estimation of global urban land cover. In: Transp. Res. Procedia, World Conference on Transport Research - WCTR 2016 Shanghai, vol. 25, pp. 3161–3173. https://doi.org/10.1016/j.trpro.2017.05.358, 10-15 July 2016.
Kohavi, R., 1995. A Study of Cross-validation and Bootstrap for Accuracy Estimation and Model Selection.
Kontgis, C., Schneider, A., Fox, J., Saksena, S., Spencer, J.H., Castrence, M., 2014. Monitoring peri-urbanization in the greater Ho Chi Minh City metropolitan area. Appl. Geogr. 53, 377–388. https://doi.org/10.1016/j.apgeog.2014.06.029.
Koppel, K., Zalite, K., Sisas, A., Voormansik, K., Praks, J., Noorma, M., 2015. Sentinel-1 for urban area monitoring #x2014; Analysing local-area statistics and interferometric coherence methods for buildings' detection. In: 2015 IEEE International Geoscience and Remote Sensing Symposium (IGARSS). Presented at the 2015 IEEE International Geoscience and Remote Sensing Symposium (IGARSS), pp. 1175–1178. https://doi.org/10.1109/IGARSS.2015.7325981.
Laveesh Bhandari, Roychowdhury, K., 2011. Night Lights and Economic Activity in India: a study using DMSP-OLS night time images. Proc. Asia Pac. Adv. Netw. 32, 218–236.
Lee, S., Lathrop, R.G., 2005. Sub-pixel estimation of urban land cover components with linear mixture model analysis and Landsat Thematic Mapper imagery. Int. J. Remote Sens. 26, 4885–4905. https://doi.org/10.1080/01431160500300222.
Levin, N., Duke, Y., 2012. High spatial resolution night-time light images for demographic and socio-economic studies. Remote Sens. Environ. 119, 1–10. https://doi.org/10.1016/j.rse.2011.12.005.
Liu, Z., He, C., Zhang, Q., Huang, Q., Yang, Y., 2012. Extracting the dynamics of urban expansion in China using DMSP-OLS nighttime light data from 1992 to 2008. Landsc. Urban Plann. 106, 62–72. https://doi.org/10.1016/j.landurbplan.2012.02.013.
Lu, D., Weng, Q., 2006. Use of impervious surface in urban land-use classification. Remote Sens. Environ. 102, 146–160. https://doi.org/10.1016/j.rse.2006.02.010.
Lu, D., Weng, Q., 2007. A survey of image classification methods and techniques for improving classification performance. Int. J. Remote Sens. 28, 823–870. https://doi.org/10.1080/01431160600746456.
Lu, D., Hetrick, S., Moran, E., Li, G., 2010. Detection of urban expansion in an urban-rural landscape with multitemporal QuickBird images. J. Appl. Remote Sens. 4 https://doi.org/10.1117/1.3501124.
Lu, Z., Im, J., Rhee, J., Hodgson, M., 2014. Building type classification using spatial and landscape attributes derived from LiDAR remote sensing data. Landsc. Urban Plann. 130, 134–148. https://doi.org/10.1016/j.landurbplan.2014.07.005.
Ma, L., Li, M., Ma, X., Cheng, L., Du, P., Liu, Y., 2017. A review of supervised object-based land-cover image classification. ISPRS J. Photogrammetry Remote Sens. 130, 277–293. https://doi.org/10.1016/j.isprsjprs.2017.06.001.
Maplecroft, 2012. Climate Change Vulnerability Index 2013 – Most at Risk Cities.
McFeeters, S.K., 1996. The use of the Normalized Difference Water Index (NDWI) in the delineation of open water features. Int. J. Remote Sens. 17, 1425–1432. https://doi.org/10.1080/01431169608948714.
Meyer, W.B., B. L. Turner, I., 1992. Human population growth and global land-use/cover change. Annu. Rev. Ecol. Systemat. 23, 39–61. https://doi.org/10.1146/annurev.es.23.110192.000351.
Millard, K., Richardson, M., 2015. On the importance of training data sample selection in random forest image classification: a case study in Peatland ecosystem mapping. Rem. Sens. 7, 8489–8515. https://doi.org/10.3390/rs70708489.
Miyazaki, H., Iwao, K., Shibasaki, R., 2011. Development of a new ground truth database for global urban area mapping from a gazetteer. Remote Sens. 3, 1177–1187. https://doi.org/10.3390/rs3061177.
Momeni, R., Aplin, P., Boyd, D.S., 2016. Mapping complex urban land cover from spaceborne imagery: the influence of spatial resolution, spectral band set and classification approach. Rem. Sens. 8, 88. https://doi.org/10.3390/rs8020088.
Montgomery, M.R., 2008. The urban transformation of the developing world. Science 319, 761–764. https://doi.org/10.1126/science.1153012.
Moreira, A., Prats-Iraola, P., Younis, M., Krieger, G., Hajnsek, I., Papathanassiou, K.P., 2013. A tutorial on synthetic aperture radar. IEEE Geosci. Remote Sens. Magn. 1, 6–43. https://doi.org/10.1109/MGRS.2013.2248301.
Nettleton, D.F., Orriols-Puig, A., Fornells, A., 2010. A study of the effect of different types of noise on the precision of supervised learning techniques. Artif. Intell. Rev. 33, 275–306. https://doi.org/10.1007/s10462-010-9156-z.
Nguyen, T.B., Samsura, D.A.A., van der Krabben, E., Le, A.-D., 2016. Saigon-Ho Chi Minh city. Cities 50, 16–27. https://doi.org/10.1016/j.cities.2015.08.007.
Oltra-Carrió, R., Briottet, X., Bonhomme, M., 2015. Impact of spatial and spectral resolutions on the classification of urban areas. In: 2015 Joint Urban Remote Sensing Event (JURSE). Presented at the 2015 Joint Urban Remote Sensing Event (JURSE), pp. 1–4. https://doi.org/10.1109/JURSE.2015.7120509.
Openshaw, Stan, Openshaw, S., 1984. The Modifiable Areal Unit Problem, Geo Abstracts. University of East Anglia.
Pandey, B., Joshi, P.K., Seto, K.C., 2013. Monitoring urbanization dynamics in India using DMSP/OLS night time lights and SPOT-VGT data. Int. J. Appl. Earth Obs. Geoinf. 23, 49–61. https://doi.org/10.1016/j.jag.2012.11.005.
Patel, N.N., Angiuli, E., Gamba, P., Gaughan, A., Lisini, G., Stevens, F.R., Tatem, A.J., Trianni, G., 2015. Multitemporal settlement and population mapping from Landsat using Google Earth Engine. Int. J. Appl. Earth Obs. Geoinf. 35 (Part B), 199–208. https://doi.org/10.1016/j.jag.2014.09.005.
Patino, J.E., Duque, J.C., 2013. A review of regional science applications of satellite remote sensing in urban settings. Comput. Environ. Urban Syst. 37, 1–17. https://doi.org/10.1016/j.compenvurbsys.2012.06.003.
Pekel, J.-F., Cottam, A., Gorelick, N., Belward, A.S., 2016. High-resolution mapping of global surface water and its long-term changes. Nature 540, 418–422. https://doi.org/10.1038/nature20584.
Pelletier, C., Valero, S., Inglada, J., Champion, N., Dedieu, G., 2016. Assessing the robustness of Random Forests to map land cover with high resolution satellite image time series over large areas. Remote Sens. Environ. 187, 156–168. https://doi.org/10.1016/j.rse.2016.10.010.
Pelletier, C., Valero, S., Inglada, J., Champion, N., Marais Sicre, C., Dedieu, G., 2017. Effect of training class label noise on classification performances for land cover mapping with satellite image time series. Rem. Sens. 9, 173. https://doi.org/10.3390/rs9020173.
Pesaresi, M., Huadong, G., Blaes, X., Ehrlich, D., Ferri, S., Gueguen, L., Halkia, M., Kauffmann, M., Kemper, T., Lu, L., Marin-Herrera, M.A., Ouzounis, G.K., Scavazzon, M., Soille, P., Syrris, V., Zanchetta, L., 2013. A global human settlement layer from optical HR/VHR RS data: concept and first results. IEEE J. Sel. Top. Appl. Earth Obs. Remote Sens. 6, 2102–2131. https://doi.org/10.1109/JSTARS.2013.2271445.
Pesaresi, M., Corbane, C., Julea, A., Florczyk, A.J., Syrris, V., Soille, P., 2016a. Assessment of the added-value of Sentinel-2 for detecting built-up areas. Rem. Sens. 8, 299. https://doi.org/10.3390/rs8040299.
Pesaresi, M., Ehrlich, Daniele, Ferri, Stefano, Florczyk, Aneta, Carneiro Freire, Sergio Manuel, Halkia, Stamatia, Julea, Andreea Maria, Kemper, Thomas, Soille, Pierre, Syrris, Vasileios, 2016b. Operating Procedure for the Production of the Global Human Settlement Layer from Landsat Data of the Epochs 1975, 1990, 2000, and 2014. Publications Office of the European Union, Ispra (VA), Italy.
Pettorelli, N., Vik, J.O., Mysterud, A., Gaillard, J.-M., Tucker, C.J., Stenseth, N.C., 2005. Using the satellite-derived NDVI to assess ecological responses to environmental change. Trends Ecol. Evol. 20, 503–510. https://doi.org/10.1016/j.tree.2005.05.011.
Pham, H.M., Yamaguchi, Y., 2011. Urban growth and change analysis using remote sensing and spatial metrics from 1975 to 2003 for Hanoi, Vietnam. Int. J. Remote Sens. 32, 1901–1915. https://doi.org/10.1080/01431161003639652.
Pham, V.C., Pham, T.-T.-H., Tong, T.H.A., Nguyen, T.T.H., Pham, N.H., 2015. The conversion of agricultural land in the peri-urban areas of Hanoi (Vietnam): patterns in space and time. J. Land Use Sci. 10, 224–242. https://doi.org/10.1080/1747423X.2014.884643.
Pohl, C., Genderen, J.L.V., 1998. Review article Multisensor image fusion in remote sensing: concepts, methods and applications. Int. J. Remote Sens. 19, 823–854. https://doi.org/10.1080/014311698215748.
Potere, D., Schneider, A., Angel, S., Civco, D.L., 2009. Mapping urban areas on a global scale: which of the eight maps now available is more accurate? Int. J. Remote Sens. 30, 6531–6558. https://doi.org/10.1080/01431160903121134.
Prasad, A.M., Iverson, L.R., Liaw, A., 2006. Newer classification and regression tree techniques: bagging and random forests for ecological prediction. Ecosystems 9, 181–199. https://doi.org/10.1007/s10021-005-0054-1.
Quang Hien, T., Cai Xue, M., Li Yuan, H., 2015. Techniques of surveying and cadastral mapping in Vietnam. Int. J. Sci. Res. Publ. 5, 1–7.
Rahman, A., Aggarwal, S.P., Netzband, M., Fazal, S., 2011. Monitoring urban sprawl using remote sensing and GIS techniques of a fast growing urban centre, India. IEEE J. Sel. Top. Appl. Earth Obs. Remote Sens. 4, 56–64. https://doi.org/10.1109/JSTARS.2010.2084072.
Rashed, T., Jürgens, C., 2010. Remote Sensing of Urban and Suburban Areas. Springer Science & Business Media.
Refaeilzadeh, P., Tang, L., Liu, H., 2009. Cross-validation. In: Liu, L., Özsu, M.T. (Eds.), Encyclopedia of Database Systems. Springer US, pp. 532–538. https://doi.org/10.1007/978-0-387-39940-9_565.
Rodriguez, J.D., Perez, A., Lozano, J.A., 2010. Sensitivity analysis of k-fold cross validation in prediction error estimation. IEEE Trans. Pattern Anal. Mach. Intell. 32, 569–575. https://doi.org/10.1109/TPAMI.2009.187.

Rodriguez-Galiano, V.F., Ghimire, B., Rogan, J., Chica-Olmo, M., Rigol-Sanchez, J.P., 2012. An assessment of the effectiveness of a random forest classifier for land-cover classification. ISPRS J. Photogrammetry Remote Sens. 67, 93–104. https://doi.org/10.1016/j.isprsjprs.2011.11.002.

Rotem-Mindali, O., Michael, Y., Helman, D., Lensky, I.M., 2015. The role of local land-use on the urban heat island effect of Tel Aviv as assessed from satellite remote sensing. Appl. Geogr. 56, 145–153. https://doi.org/10.1016/j.apgeog.2014.11.023.

Roth, M., Oke, T.R., Emery, W.J., 1989. Satellite-derived urban heat islands from three coastal cities and the utilization of such data in urban climatology. Int. J. Remote Sens. 10, 1699–1720. https://doi.org/10.1080/01431168908904002.

Saksena, S., Fox, J., Spencer, J., Castrence, M., DiGregorio, M., Epprecht, M., Sultana, N., Finucane, M., Nguyen, L., Vien, T.D., 2014. Classifying and mapping the urban transition in Vietnam. Appl. Geogr. 50, 80–89. https://doi.org/10.1016/j.apgeog.2014.02.010.

Salzberg, S.L., 1997. On comparing classifiers: Pitfalls to avoid and a recommended approach. Data Min. Knowl. Discov. 1, 317–328. https://doi.org/10.1023/A:1009752403260.

Schneider, A., Friedl, M.A., Potere, D., 2010. Mapping global urban areas using MODIS 500-m data: new methods and datasets based on "urban ecoregions." Remote Sens. Environ. 114, 1733–1746. https://doi.org/10.1016/j.rse.2010.03.003.

Sertel, E., Akay, S.S., 2015. High resolution mapping of urban areas using SPOT-5 images and ancillary data. Int. J. Environ. Geoinf. 2.

Seto, K.C., Fragkias, M., Güneralp, B., Reilly, M.K., 2011. A meta-analysis of global urban land expansion. PLoS One 6, e23777. https://doi.org/10.1371/journal.pone.0023777.

Seto, K.C., Güneralp, B., Hutyra, L.R., 2012. Global forecasts of urban expansion to 2030 and direct impacts on biodiversity and carbon pools. Proc. Natl. Acad. Sci. 109, 16083–16088. https://doi.org/10.1073/pnas.1211658109.

Sharma, R.C., Hara, K., Tateishi, R., 2017. High-resolution vegetation mapping in Japan by combining Sentinel-2 and Landsat 8 based multi-temporal datasets through machine learning and cross-validation approach. Land 6, 50. https://doi.org/10.3390/land6030050.

Shi, K., Huang, C., Yu, B., Yin, B., Huang, Y., Wu, J., 2014a. Evaluation of NPP-VIIRS night-time light composite data for extracting built-up urban areas. Remote Sens. Lett. 5, 358–366. https://doi.org/10.1080/2150704X.2014.905728.

Shi, W., Miao, Z., Debayle, J., 2014b. An integrated method for urban main-road centerline extraction from optical remotely sensed imagery. IEEE Trans. Geosci. Rem. Sens. 52, 3359–3372. https://doi.org/10.1109/TGRS.2013.2272593.

Slonecker, E.T., Jennings, D.B., Garofalo, D., 2001. Remote sensing of impervious surfaces: a review. Remote Sens. Rev. 20, 227–255. https://doi.org/10.1080/02757250109532436.

Small, C., 2016. Projecting the urban future: contributions from remote sensing. Spat. Demogr. 4, 17–37. https://doi.org/10.1007/s40980-015-0002-4.

Small, C., Elvidge, C.D., 2013. Night on Earth: mapping decadal changes of anthropogenic night light in Asia. Int. J. Appl. Earth Obs. Geoinf. Spat. Stat. Mapp. Environ. 22, 40–52. https://doi.org/10.1016/j.jag.2012.02.009.

Small, C., Elvidge, C.D., Baugh, K., 2013. Mapping urban structure and spatial connectivity with VIIRS and OLS night light imagery. In: joint Urban Remote Sensing Event 2013. Presented at the Joint Urban Remote Sensing Event 2013, pp. 230–233. https://doi.org/10.1109/JURSE.2013.6550707.

Son, N.-T., Chen, C.-F., Chang, L.-Y., Chen, C.-R., Thanh, B.-X., 2012. Urban growth mapping from Landsat data using linear mixture model in Ho Chi Minh City. Vietnam. J. Appl. Remote Sens. 6, 063543 https://doi.org/10.1117/1.JRS.6.063543.

Stevens, F.R., Gaughan, A.E., Linard, C., Tatem, A.J., 2015. Disaggregating census data for population mapping using random forests with remotely-sensed and ancillary data. PLoS One 10, e0107042. https://doi.org/10.1371/journal.pone.0107042.

Su, Y., Chen, X., Wang, Chongyang, Zhang, H., Liao, J., Ye, Y., Wang, Changjian, 2015. A new method for extracting built-up urban areas using DMSP-OLS nighttime stable lights: a case study in the Pearl River Delta, Southern China. GIScience Remote Sens. 52, 218–238. https://doi.org/10.1080/15481603.2015.1007778.

Sudhira, H.S., Ramachandra, T.V., Jagadish, K.S., 2004. Urban sprawl: metrics, dynamics and modelling using GIS. Int. J. Appl. Earth Obs. Geoinf. 5, 29–39. https://doi.org/10.1016/j.jag.2003.08.002.

Sutton, P.C., 2003. A scale-adjusted measure of "Urban sprawl" using nighttime satellite imagery. Remote Sens. Environ. Urban Remote Sens. 86, 353–369. https://doi.org/10.1016/S0034-4257(03)00078-6.

Swetnam, R.D., Fisher, B., Mbilinyi, B.P., Munishi, P.K.T., Willcock, S., Ricketts, T., Mwakalila, S., Balmford, A., Burgess, N.D., Marshall, A.R., Lewis, S.L., 2011. Mapping socio-economic scenarios of land cover change: a GIS method to enable ecosystem service modelling. J. Environ. Manag. 92, 563–574. https://doi.org/10.1016/j.jenvman.2010.09.007.

Taubenböck, H., Kraff, N.J., 2014. The physical face of slums: a structural comparison of slums in Mumbai, India, based on remotely sensed data. J. Hous. Built Environ. 29, 15–38. https://doi.org/10.1007/s10901-013-9333-x.

Taubenböck, H., Esch, T., Felbier, A., Wiesner, M., Roth, A., Dech, S., 2012. Monitoring urbanization in mega cities from space. Remote Sens. Environ. 117, 162–176. https://doi.org/10.1016/j.rse.2011.09.015.

Trianni, G., Lisini, G., Angiuli, E., Moreno, E.A., Dondi, P., Gaggia, A., Gamba, P., 2015. Scaling up to national/regional urban extent mapping using Landsat data. IEEE J. Sel. Top. Appl. Earth Obs. Remote Sens. 8, 3710–3719. https://doi.org/10.1109/JSTARS.2015.2398032.

Triet, L., Phu, V., 2014. Project Report on Assessment of Impacts of Climate Change on Flowrate, Water Quality and Salinity Intrusion of Saigon River and Proposal of Adaptation Measures. Dept of Science and Technology, HCMC, Ho Chi Minh City, Vietnam.

Trincsi, K., Pham, T.-T.-H., Turner, S., 2014. Mapping mountain diversity: ethnic minorities and land use land cover change in Vietnam's borderlands. Land Use Pol. 41, 484–497. https://doi.org/10.1016/j.landusepol.2014.06.022.

UN, 2006. World Urbanization Prospects, the 2005 Revision. Department of Economic and Social Affairs, Population Division, New York.

UN, 2014. World Urbanization Prospects: the 2014 Revision (No. ST/ESA/SER.A/352).

van Dijk, M., Hilderink, H., van Rooij, W., Rutten, M., Ashton, R., Kartikasari, K., Vu Cong, L., 2013. Land-use Change, Food Security and Climate Change in Vietnam; a Global-to-local Modelling Approach (No. LEI Report 2013-020). LEI Wageningen UR The Hague.

Venables, A.J., 2017. Breaking into tradables: urban form and urban function in a developing city. J. Urban Econ. Urban. Develop. Countries: Past Present 98, 88–97. https://doi.org/10.1016/j.jue.2017.01.002.

Vietnam Urbanization Review: Technical Assistance Report (No. P122324), 2011. Cities Alliance Project Output. World Bank.

Wan, B., Guo, Q., Fang, F., Su, Y., Wang, R., 2015. Mapping US urban extents from MODIS data using one-class classification method. Rem. Sens. 7, 10143–10163. https://doi.org/10.3390/rs70810143.

Wang, Q., Blackburn, G.A., Onojeghuo, A.O., Dash, J., Zhou, L., Zhang, Y., Atkinson, P.M., 2017. Fusion of Landsat 8 OLI and Sentinel-2 MSI data. IEEE Trans. Geosci. Rem. Sens. 55, 3885–3899. https://doi.org/10.1109/TGRS.2017.2683444.

Weng, Q., 2012. Remote sensing of impervious surfaces in the urban areas: requirements, methods, and trends. Remote Sens. Environ. Remote Sens. Urban Environ. 117, 34–49. https://doi.org/10.1016/j.rse.2011.02.030.

Xiao, P., Wang, X., Feng, X., Zhang, X., Yang, Y., 2014. Detecting China #x2019;s urban expansion over the past three decades using nighttime light data. IEEE J. Sel. Top. Appl. Earth Obs. Remote Sens. 7, 4095–4106. https://doi.org/10.1109/JSTARS.2014.2302855.

Yin, Z.-Y., Stewart, D.J., Bullard, S., MacLachlan, J.T., 2005. Changes in urban built-up surface and population distribution patterns during 1986–1999: a case study of Cairo, Egypt. Comput. Environ. Urban Syst., Remote Sens. Urban Anal. 29, 595–616. https://doi.org/10.1016/j.compenvurbsys.2005.01.008.

Yue, W., Liu, Y., Fan, P., 2013. Measuring urban sprawl and its drivers in large Chinese cities: the case of Hangzhou. Land Use Pol. 31, 358–370. https://doi.org/10.1016/j.landusepol.2012.07.018. Themed Issue 1-Guest Editor Romy GreinerThemed Issue 2- Guest Editor Davide Viaggi.

Zeng, C., Wang, J., Lehrbass, B., 2013. An evaluation system for building footprint extraction from remotely sensed data. IEEE J. Sel. Top. Appl. Earth Obs. Remote Sens. 6, 1640–1652. https://doi.org/10.1109/JSTARS.2013.2256882.

Zha, Y., Gao, J., Ni, S., 2003. Use of normalized difference built-up index in automatically mapping urban areas from TM imagery. Int. J. Remote Sens. 24, 583–594. https://doi.org/10.1080/01431160304987.

Zhang, Q., Seto, K.C., 2011. Mapping urbanization dynamics at regional and global scales using multi-temporal DMSP/OLS nighttime light data. Remote Sens. Environ. 115, 2320–2329. https://doi.org/10.1016/j.rse.2011.04.032.

Zhang, Q., Seto, K.C., 2013. Can night-time light data identify typologies of Urbanization? A global assessment of successes and failures. Rem. Sens. 5, 3476–3494. https://doi.org/10.3390/rs5073476.

Zhang, Q., Wang, J., Peng, X., Gong, P., Shi, P., 2002. Urban built-up land change detection with road density and spectral information from multi-temporal Landsat TM data. Int. J. Remote Sens. 23, 3057–3078. https://doi.org/10.1080/01431160110104728.

Zhang, H., Zhang, Y., Lin, H., 2012. Urban land cover mapping using random forest combined with optical and SAR data. In: 2012 IEEE International Geoscience and Remote Sensing Symposium. Presented at the 2012 IEEE International Geoscience and Remote Sensing Symposium, pp. 6809–6812. https://doi.org/10.1109/IGARSS.2012.6352600.

Ziegler, A.D., Giambelluca, T.W., Plondke, D., Leisz, S., Tran, L.T., Fox, J., Nullet, M.A., Vogler, J.B., Minh Troung, D., Vien, Tran Duc, 2007. Hydrological consequences of landscape fragmentation in mountainous northern Vietnam: buffering of Hortonian overland flow. J. Hydrol 337, 52–67. https://doi.org/10.1016/j.jhydrol.2007.01.031.